THESIS

DC ELECTRICAL RESITIVITY CONSTRAINTS ON HYDROSTRATIGRAPHY IN THE LOWER SOUTH PLATTE RIVER ALLUVIAL AQUIFER IN NORTHEASTERN COLORADO

Submitted by

Reece Lonsert

Department of Geosciences

In partial fulfillment of the requirements

For the Degree of Master of Science

Colorado State University

Fort Collins, Colorado

Summer 2013

Master's Committee:

Advisor: Dennis Harry

John Stednick
Michael Ronayne

ABSTRACT

DC ELECTRICAL RESITIVITY CONSTRAINTS ON HYDROSTRATIGRAPHY IN THE LOWER SOUTH PLATTE RIVER ALLUVIAL AQUIFER IN NORTHEASTERN COLORADO

This study uses DC Electrical Resistivity Tomography (ERT) to delineate hydrostratigraphic units within the lower South Platte River alluvial aquifer. The geophysical investigation was conducted at Tamarack Ranch State Wildlife Area in northeastern Colorado, where the South Platte River is artificially recharged via pumping to surface recharge ponds and groundwater flow through the underlying unconfined alluvial aquifer system. Twenty-seven ERT profiles collected within a 4.2 km^2 study area on the south bank of the South Platte River define 3 different electrostratigraphic units. The ERT data was correlated with drilling logs and laboratory resistivity measurements to develop a hydrostratigraphic model and confining bedrock surface map. Results indicate 7-25 m thick eolian sand deposits (50-800 ohm-m) serve as infiltration zones and do not readily store groundwater. These eolian deposits form up to 15 m high sand hills in the southern half of the study area, and underlie recharge ponds that are used as water sources for artificial recharge of the river. The underlying alluvium (20-3890 ohm-m) varies from 10-70 m thick and functions as the primary groundwater storage unit. A 10-20 m thick intermittent conductive zone (25-80 ohm-m) occurs within the upper part of the alluvial layer that underlies the sand hills, and is interpreted to be caused by clay deposits that potentially influence initial groundwater flow paths emanating from the recharge ponds. The alluvium is underlain by highly conductive siltstone and claystone bedrock formations (1-60 ohm-m) that confine the aquifer system. The bedrock surface is complexly eroded (1055-1110 m.a.s.l.) and is characterized by prominent large-scale paleo-topographic lows (at typical scales of 700 m wide, 35-40 m deep and 700 m wide, 20-25 m deep) that occur on the northern bank of an incised paleo-channel. These features are interpreted to represent a paleo-topographic surface formed by groundwater outflow in the form of piping and sapping networks. The rugged bedrock topography establishes a previously unrecognized first order control on groundwater flowpaths within the unconfined alluvial aquifer.

ACKNOWLEDGEMENTS

I would like to express my sincere gratitude to my advisor, Dennis Harry, for showing me the world through the eyes of a geophysicist and teaching me a valuable suite of skills that will allow me to succeed as a professional. The completion of this project is greatly credited to his patience, availability, feedback, and encouragement. I would also like to thank John Stednick and Michael Ronayne for representation on my graduate committee and for their willingness to help me understand the complexities of groundwater processes. Finally, I could not have accomplished this research without the tremendous effort of my field assistant Alan Lewis, thank you for your countless hours of help in tick-infested fields.

TABLE OF CONTENTS

LIST OF FIGURES

1. Introduction

In the United States, sand and gravel aquifers are vital water resources that account for 80 percent of groundwater supply [Maupin and Barber, 2005]. These largely unconfined aquifer systems have been used extensively for agricultural purposes, especially the High Plains aquifer of the North American Great Plains (Fig. 1). This regionally extensive aquifer accounts for nearly 30 percent of total groundwater withdrawals from sand and gravel aquifers in the U.S. with 97 percent of the pumped water for irrigation [Maupin and Barber, 2005]. Within the past century, intensive groundwater pumping has depleted approximately 8 percent of the High Plains aquifer [McGuire, 2013]. Continual over withdrawal in the High Plains aquifer is a major concern and has become a trend observed in aquifers across the U.S. that must be addressed in order to protect important groundwater resources from further depletion (Barber, 2009). Implementing more efficient groundwater management practices will require a more detailed study of aquifer properties at the local and regional scale. This information can optimize current and future induced recharge operations, which have become increasingly necessary to manage growing human populations that continue to stress finite water resources [Bouwer, 2002].

Within the past few decades, the state of Colorado has engineered artificial recharge systems along the South Platte River Valley to meet increasing water demands [Bredehoeft, 2011]. These operations serve to recharge the aquifer by capturing surplus winter and spring flows. This study was undertaken at Tamarack Ranch State Wildlife Area (Tamarack), an artificial recharge site situated within the lower South Platte River alluvial aquifer in northeastern Colorado that is hydraulically connected and westerly adjacent to the High Plains aquifer (Figs. 2 and 3). The site operates pumping wells from February to May, capturing excess flows at times when there are no calls on the river. Groundwater is extracted from the aquifer near the South Platte River and pumped to recharge ponds situated in upland eolian sand deposits (Fig. 3). The intent is for artificial recharge to occur as pumped water enters back into the unconfined aquifer system and returns to the river during the late summer months when stream flows are low.

The artificial recharge project at Tamarack was developed as part of the Platte River Recovery and Implementation Program (PRRIP) which was established in 2006 to help fulfill Colorado's role in the Three States Cooperative Agreement of 1997 with Wyoming, Nebraska, and the Department of the Interior. The primary focus of PRRIP is to create and maintain critical aquatic habitats in the Central Platte River Basin for federally endangered (whooping crane, interior least tern, and pallid sturgeon) and threatened species (piping plover) protected under the

Endangered Species Act. This has been accomplished in part through induced groundwater recharge at Tamarack, where re-timing excess flows has provided increased in-stream flows to Nebraska during the late summer months when aquatic habitats are stressed.

Accurately mapping hydrostratigraphic units that comprise the overall structure of an unconfined aquifer, especially confining aquifer unit geometry, is fundamental to the development and management of artificial recharge operations. A thorough understanding of confining bedrock topography is required to define an aquifer's areal extent, thickness, volume, and hydraulic connectivity to adjacent aquifers [Tait et al., 2004, Srivastava, 2005; Samadder et al., 2007, Samadder et al., 2011]. A bedrock map of the regionally extensive High Plains aquifer developed from lithological and geophysical logs from thousands of water wells and test wells in parts of Colorado, Kansas, Nebraska, New Mexico, Oklahoma, South Dakota, Texas, and Wyoming reveals a generally easterly dipping surface on which the aquifer was deposited [Weeks and Gutentag, 1981]. However, due to the distribution of data, the regional bedrock surface does not detail the morphology of the complex and intricately sculpted topographic surface that likely underlies the High Plains aquifer [Weeks and Gutentag, 1981]. Similarly, the regional bedrock surface of the South Platte Alluvial aquifer has been constrained by data collected from numerous wells across Colorado [Hurr et al., 1972; Hurr et al., 1973a, 1973b, 1973c, 1973d]. The purpose of this study is to assess the structure and geometry of the unconfined South Platte Alluvial aquifer on a more local and detailed scale than previous studies. To accomplish this, we use surface DC electrical Resistivity surveys to develop tomographic models of the subsurface resistivity structure that provide new information to constrain the thickness, nature, and spatial distribution of hydrostratigraphic units that facilitate groundwater flow through the aquifer. We focus particularly on paleo-topographic features on the confining aquifer unit that potentially exist at a regional scale and are likely to play a key role in groundwater flow.

The confining unit beneath the unconfined alluvial aquifer in the South Platte River Valley within the study area is largely comprised of the Tertiary White River Group. The White River Group is the basal unit for 28 percent of the High Plains aquifer system in Colorado, Nebraska, Wyoming, and South Dakota and a portion of the South Platte River Valley alluvial aquifer in northeastern Colorado (Fig. 2) [Bjorkland and Brown, 1957; Weeks and Gutentag, 1981]. The White River Group is largely characterized by poorly cemented beds of clay and silt, which easily erode and are highly susceptible to mass wasting processes [Graham, 2008]. Consequently, outcrops typically consist of steeply sloping features in the form of bluffs, buttes, gulches, valley walls, spired structures, and other heavily eroded structures [Henderson, 1907; Barrash and Morin, 1987; Terry, 1998]. Limited bedrock exposures are scattered across the northern Great Plains, outcropping in Colorado, Nebraska, Wyoming, South Dakota, and North Dakota (Fig. 2). The most notable outcrops comprise Badlands National Park, South Dakota (Fig. 2), where the term badland topography was coined to describe similar heavily eroded areas formed on weakly consolidated fine-grained sediments. Although these exposures represent a small fraction of the regionally extensive White River Group, structures similar to these outcrops potentially comprise aerially extensive buried paleo-landscapes that underlie shallow aquifer systems throughout the northern Great Plains.

2. Site Description

Tamarack is located within the lower South Platte River Valley, southeast from the town of Crook in Logan County, Colorado. The 4.2 km^2 study site is situated on the flood plain of the braided South Platte River and adjacent eolian sand hills, where the South Platte River is recharged via groundwater flow through the underlying unconfined aquifer system (Figs. 2 and 3). A series of conformable and unconformable strata serve as principal hydrostratigraphic units that influence groundwater flow within the unconfined aquifer system (Fig. 4). Pleistocene eolian sand deposits form gentle hills south of the river that rise up to 15 m above the surface of the South Platte River. These highly permeable sand deposits are largely composed of very fine to medium grained sand and serve as good infiltration zones for groundwater recharge [Bjorkland and Brown, 1957; Waltz, 1972]. Grain-size analyses conducted on four surface samples indicate the eolian deposits consist of 33-35% medium sand, 33-36% fine sand, 13-15% coarse sand, 8-10% very fine sand, and 5-7% silts and clays.

Early Pleistocene to recent alluvium extends southeast from the river as a floodplain to the base of the sand hills and conformably underlies the eolian deposits. The alluvium ranges from well sorted to poorly sorted, consisting of mixtures of gravel, sand, and clay with lenses of these materials existing as aggraded channel deposits of the South Platte River [Bjorkland and Brown, 1957]. Grain-size analyses of subsurface samples taken from two piezometer nests describe heterogeneous alluvial sediments consisting of 18-23% very fine gravel, 17-22% coarse sand, 17-20% very coarse sand, 13-19% medium sand, 13-19% fine gravel, 5-8% fine sand, 2-5% medium gravel, 0-1% very fine sand, and 0-1% silts and clays. The alluvium serves as the primary aquifer unit that is hydraulically connected to the South Platte River, receiving infiltrating waters from the overlying eolian sand deposits.

A regional paleo-river valley cuts into formations of the confining aquifer unit with alluvium thicknesses ranging from 2 m near the edge of the river, to almost 90 m in the center of the paleo-valley [Bjorkland and Brown, 1957; Warner et al., 1994].The confining unit is comprised of fine-grained strata of the Tertiary White River Group and the upper Cretaceous Pierre Shale Formation. The White River Group consists of the Brule Formation of Early Oligocene age underlain by the conformable Chadron Formation of Late Eocene age. Significant volumes (~60%) of eolian volcaniclastic materials, primarily ash, characterize the White River Group, with the largest fraction (>80%) occurring in the upper Brule Formation [Larson and Evanoff, 1998; Condon, 2005]. The Brule Formation is a massive siltstone with a regionally uniform grain-size distribution comprised of 65-85% silt, 10-20% clay, and 5-25% very fine sand [Barrash and Morin, 1987]. Heterogeneities within the Brule Formation include localized beds of clays, tuffs, ash, and fine-grained sands, as well as coarser channel-fill deposits and sandstone beds [Bjorkland and Brown, 1957; Weeks and Gutenatg, 1981; Larson and Evanoff, 1998]. The Brule Formation fractures readily into blocky fragments and interconnected bedrock. Extensive fracture zones and coarser more porous deposits form flow pathways that provide adequate groundwater yields in regions within the High Plains aquifer [Bjorkland and Brown, 1957; Weeks and Gutentag, 1981; Barrash and Morin, 1987].

The underlying Chadron Formation largely consists of bentonitic clays and silts containing numerous sand and gravel channel deposits throughout the formation that occur more frequently near the upper and lower boundaries [Bjorkland and Brown, 1957]. The Chadron and Pierre Formations are associated with high swelling clay contents capable of storing large volumes of water, but are not recognized to yield appreciable quantities of extractable water [Bjorkland and Brown, 1957; Graham, 2008; Anderson et al., 2009]. The unconformable Pierre Formation that underlies the White River Group consists of a predominately massive marine shale unit that contains sands as well as limestone layers in the upper transition zone [Bjorkland and Brown, 1957].

Previous subsurface mapping studies undertaken by Hurr et al. [1972; 1973a, 1973b, 1973c, 1973d] utilized borehole data within the South Platte River Valley to constrain the regional bedrock configuration. Their results indicated an incised paleo-channel that cuts into the confining unit, deepening eastward from Greeley to Julesburg, Colorado (Fig. 2). This former river channel functions as the dominant paleo-feature influencing groundwater flow paths in the South Platte alluvial aquifer system. Within the Tamarack Ranch State Wildlife Area, the incised channel is characterized by an easterly-northeasterly trend, moderately steep banks, and a flat channel bottom that widens from 600 m to 1000 m toward the northeast, (Fig. 5) [Hurr et al. 1973a].

3. Data acquisition and processing

Methods used in this study include surface direct current (DC) electrical resistivity tomography (ERT) and laboratory resistivity measurements. ERT is used to differentiate saturated and unsaturated sediments, detect the vertical and lateral extents of sand and alluvial deposits, and identify highly conductive fine-grained strata such as clays and siltstones [e.g., Lucius et al., 2007]. Resistivity of each litho-facies present in the study area was measured in the laboratory in order to relate subsurface resistivities and structure observed in the ERT data to lithology and subsurface water content.

3.1 Electrical Resistivity Tomography Profiles

Our geophysical surveys were undertaken in April and May of 2012. Groundwater was pumped continuously throughout the majority of data collection. We expect profiles were recorded under equivalent hydrologic conditions and the ERT data represent changes in lithology and subsurface water content and does not reflect time-varying aquifer conditions. The Tamarack survey design included twenty-seven DC electrical resistivity profiles, which varied from 230 m to 1190 m in length and were oriented approximately parallel and perpendicular to the South Platte River (Fig. 3). Data were collected using a 48 electrode Iris Syscal Pro system and a two dimensional dipole-dipole array. A roll-along technique was used to extend profiles that spanned distances greater than that covered by the 48 electrodes available for the survey. The dipole-dipole array was chosen for its ample penetration depth and vertical resolution [Dahlin and Zhou, 2004]. Multiple voltage measurements were recorded for each offset between potential and injection electrode pairs with the voltage drop between potential electrodes set to a constant 400 V. The majority of survey lines used a 10 m electrode spacing (5 m spacing was used where space prohibited longer offsets) with a maximum offset of 160 m.

Geotomo Inc.'s RES2DINV© software was used to generate 2D subsurface resistivity profiles from the surface voltage measurements via tomographic inversion [Loke and Dahlin, 2002]. The subsurface was discretized into a grid of model cells spanning the length of the survey lines and extending from the surface to depths ranging from 55-130 m. Model cells have thicknesses ranging from approximately 2-4 m in the top row of cells depending on electrode spacing to approximately 13 m in the bottom row. Cell widths equal the electrode spacing. Topographic data was extracted from 1/3-arcsecond digital elevation models (DEM) that corresponded to GPS locations taken during surveying [Gesch, 2007]. The tomographic inversion in RES2DINV© is based on a finite element forward model that calculates voltages at each surface electrode location based on the known electrode array and a modeled subsurface resistivity structure [Loke and Barker, 1996; Loke and Dahlin, 2002]. Initially, a constant resistivity is assumed for the subsurface, equal to the average apparent resistivity measured for the profile. The resistivity in each model cell is then iteratively modified using a Gauss-Newton least-squares algorithm to minimize the misfit between the modeled and observed voltage drops for each electrode pair. The robust inversion method (l_1-norm) was selected as the misfit measure to be minimized in order to reduce the influence of outliers in comparison to higher order norms and to promote sharp model boundaries between distinct resistivity units, such as is anticipated to be present on the confining bedrock surface [Loke et al. 2003].

Prior to inversion, noisy data points were eliminated on the basis of three criteria. First, voltage measurements that differed less than 5% from the recorded self-potential were eliminated. These data points typically corresponded to weak signal strength or poorly coupled electrodes. Secondly, data from electrode pair combinations with measurement standard deviations greater than 0.5% were removed. Lastly, data with apparent resistivity differing by more than approximately 80% from their neighboring five measurements were eliminated. The data removed from each profile ranged between 0-27.8% of the measurements, averaging 8.4% for the twenty-seven profiles, which is typical for resistivity modeling.

Depth of investigation (DOI) tests were conducted to examine the reliability of our inverted resistivity models [Oldenburg and Li, 1999]. To estimate the DOI, two separate inversions were carried on the same dataset using two different reference models (keeping all other inversion parameters the same). The reference model is heavily weighted during the inversion, so that the final model matches the reference model in areas where the subsurface resistivity is poorly constrained by the data. For the first inversion, the reference model is a constant resistivity equal to one tenth of the average apparent resistivity. In the second inversion, the reference model is ten times the average apparent resistivity. A DOI index is calculated for each model cell by dividing the difference of the generated model cell resistivity values, obtained from the first and second inversions by the difference of the first and second constant reference model cell resistivity values. Small DOI indices characterize well-constrained model regions that yield the same model cell resistivity regardless of the reference model, whereas large DOI indices indicate poorly constrained regions that default to cell resistivities similar to the reference model. DOI results were integrated into final resistivity models by removing poorly constrained model cells with normalized DOI indices greater than 0.1 [Oldenburg and Li, 1999].

3.2 Laboratory Resistivity Measurements

Resistivity measurements were conducted on eolian sand samples collected near the recharge pond and on alluvium and bedrock samples obtained from piezometer nest drill tailings. Alluvial and eolian samples were tested to determine resistivity with respect to water content and lithology. Measurements were taken on samples associated with specified gravimetric water content (w), equal to the mass of water divided by the mass of dry sample (w = 0.03, 0.06, 0.09, 0.12, 0.15, and 0.20). The water contents measured were chosen to span the range from dry sediment to saturation corresponding to the maximum measured water holding capacity for the eolian and alluvial sediments (w = 0.20 and w = 0.15, respectively).   Saturated claystone bedrock samples of the Chadron Formation were placed in airtight bags and frozen to preserve *in situ* water content and inhibit microorganism growth. Resistivity measurements were taken on water logged samples once they had been brought to room temperature. Following resistivity measurements, samples were dried and the stored gravimetric water content was calculated as w = 0.25.

The laboratory resistivity measurements followed a similar setup described by Telford et al. [1990]. Eolian and alluvial samples were packed into a plastic cylinder and clay samples were molded into cylindrical shape. Copper end plates were placed at the ends of the samples, and a uniform DC electrical current was passed through the system. Using Ohm's Law (I = V/R), current (I) was calculated by measuring the voltage drop (V) across a 22 k-ohm resistor in series with the sample. Sample resistance (R) is determined by dividing the known current by the measured voltage drop (V) between the copper end plates. Finally, sample resistivity (ρ) was obtained from;

$$\rho = \frac{V}{I} \cdot \frac{A}{L} = R \cdot \frac{A}{L}$$

where (A) is the cross sectional area of the copper plates and (L) is the length of the sample [Telford, 1990].

4. Data analysis and interpretation

The final subsurface resistivity models required between 3-5 iterations during the inversion, with RMS error values ranging from 1.98-10.19% (the average RMS error is 5.33% for all models). The major features discussed in this section are observed to be robust, appearing in numerous inverted tomograms using varying model constraints. A layered electrostratigraphic structure is observed in the ERT profiles, consisting of 3 electro-facies. The electro-facies were correlated with laboratory resistivity measurements, borehole data, and surface observations to identify and characterize the hydrostratigraphic units (Fig. 4) and to construct a bedrock surface map of the confining aquifer unit. Within the following section, explanations of significant subsurface findings always begin with the shallowest features before proceeding to the deepest. After briefly summarizing the 3 electro-facies interpreted to represent local geology, we describe laboratory resistivity results distinguishing general trends for overlapping resistivity ranges in ERT data, associated with eolian sands, alluvium, and fine-grained strata. Results from the two-dimensional profiles are further described by interpreting boundaries and heterogeneities attributed to each electro-facie. From the interpreted geophysical results we then identify structures comprising the bedrock surface.

Electro-facies 1 (EF1) is interpreted to correspond to the eolian sands which are the uppermost lithostratigraphic unit. This facies forms a 7-25 m thick layer that thins to the northwest with resistivities ranging from 50-800 ohm-m. Electro-facies 2 (EF2) defines a 10-70 m thick layer that is interpreted to represent the alluvial sediments exposed at the surface in the northern portion of the study area and underlying the eolian sand deposits in the southern area. Modeled resistivities observed in EF2 exhibit the highest variability of all the electro-facies, with values ranging from 20-3890 ohm-m. Electro-facies 3 (EF3) underlies EF2, and is interpreted to represent the fine-grained Tertiary and Cretaceous bedrock formations in the study area. EF3 is an electrically conductive layer with resistivities ranging from 1-60 ohm-m.

Results indicate eolian sand deposits are largely unsaturated. Laboratory resistivity measurements conducted on eolian samples with very low water content ($w = 0.03$) have resistivities ranging from 230-325 ohm-m (Fig. 6). The tomographic models indicate that EF1 is largely characterized by resistivities greater than 200 ohm-m (e.g., Fig. 7a and 7d, respectively). This is consistent with previous studies that have shown resistivities greater than 200 ohm-m to be characteristic of dry sands [Lucious et al., 2007]. Therefore EF1 is interpreted to represent unsaturated eolian sands.

The laboratory resistivity measurements in conjunction with ERT data suggest that the majority of the alluvial deposits are saturated. Alluvial samples corresponding to the maximum holding capacity (w = 0.15) have resistivity values ranging from 50-100 ohm-m (Fig. 6). These values fall within the expected range for saturated sands and gravels [Reynolds, 1997], and are frequently observed within EF2 (e.g., Figs. 7a-e), which is interpreted to correspond to saturated alluvial sediments.

The water holding capacity for the underlying bedrock largely depends on the presence of swelling clays. Resistivity measurements taken on the water filled clay samples (w = 0.25) range from 13-17 ohm-m (Fig. 6). This is similar to the low resistivities that largely characterize EF3 and is therefore interpreted to represent the clay-rich confining unit at Tamarack (Figs. 7a-e).

Lithological and hydrological boundaries are commonly defined by sharp resistivity gradients in the ERT data. A sharp vertical resistivity gradient underlies EF1 at depths ranging from 1120-1130 m.a.s.l. (approximately corresponding to the 100 ohm-m contour) (Fig. 7a). Water-level measurements and drilling logs in close proximity to profiles indicate this boundary correlates to the water table and the contact between eolian sands and alluvium (Poceta, 2005). Consequently, a sharp resistivity gradient (generally associated with the 100 ohm-m contour) is interpreted to typically denote the water table throughout the study area as well as the boundary between facies EF1 and EF2. In some areas, EF1 exhibits anomalously low resistivity (50-125 ohm-m), suggesting a higher moisture content in the eolian sediments. For example, a low resistivity relatively concave downward section (50-125 ohm-m) is observed in profile 1 near the surface in a topographic low, from positions 330 to 380 m (Feature A in Fig. 7a). Similar features, on the scale of 50 m to 150 m in length, are present on other profiles and also occur below topographic depressions. These areas of low resistivity are interpreted to result from natural groundwater recharge where meteoric waters seep into the groundwater system. Similarly, profiles collected near artificial recharge ponds exhibit distinctively shaped, concave upward, semi-elliptical low resistivity bodies (100 to 260 m in length) that are interpreted to represent groundwater mounds forming within eolian sand deposits that result from induced groundwater recharge (Feature A in Fig. 7d).

A relatively narrow range of resistivity values (40-100 ohm-m) distinguishes EF2 (e.g., Fig. 7b). However, distinctive resistive and conductive heterogeneities exist within this unit that are interpreted to result from lithologically variable alluvium and artificial recharge processes. Anomalously high resistivity zones, ranging from 250-3890 ohm-m and 1-20 m thick appear in profiles located near pumping wells. Examples of these features can be observed in profile 3 from 0-150 m (maximum depth of resistivity anomalies outlined in Fig. 7c). These resistivities are comparable to those measured in unsaturated alluvial sediments (Fig. 6), and are interpreted to result from groundwater drawdown as a result of pumping. The region of drawdown extends along the pumping well transect, northward to the river, and 100-130 m southward (Fig. 3). The highest resistivities in facies EF2 (1350-3890 ohm-m) occur near the river within a distinctive 5-8 m thick layer. This appears continuously across profile 5 from and corresponds to a localized coarse gravel deposit (maximum depth of resistive anomaly outlined in Fig. 7e). Smaller scale, more moderate, resistive features (120-200 ohm-m) appear within the alluvium below the water table. Based on laboratory resistivity measurements, these features indicate partially saturated alluvial deposits. Since these features appear below the water table they are interpreted to represent more compacted sediments storing less water (e.g., Feature B in profile 1 from 160-200 m with resistivities ranging from 125-180 ohm-m in Fig. 7a).

An intermittent anomalously conductive zone, with resistivities ranging from 25-80 ohm-m, lies in the upper 5-20 m of EF2 in portions of the study area where EF2 is overlain by eolian sand deposits (the areal extent of this conductive layer is outlined in Fig. 3). The moderately conductive layer is comprised of low resistivity bodies exhibiting lobate geometries that generally extend downward into the deeper part of the alluvial layer. An example is seen in profile 1, where 5-20 m thick anomalous bodies of low to moderate resistivities occur semi-continuously near the top of EF2 (maximum depth of conductive anomaly outlined in Fig. 7a and 7d, respectively). This conductive zone is considerably less pronounced in profiles furthest away from recharge ponds, suggesting the influx of pumped water in conjunction with sediment type contributes to the lower resistivities. A lithological log near profile 1 describes a 4.6 m clay layer that corresponds to the top of the conductive zone (1127 m.a.s.l.) overlying a 5.9 m interval of interbedded gravels and sands, which is underlain by a 1.5 m clay deposit. These clay and gravel layers comprise a 12 m thick section that typically corresponds to the depth dimension of the interval encompassing the low resistivity lobate bodies. At greater depths, the log shows a more heterogeneous mixture of gravels, and sands with few fines. The localized conductive zone is not present below the alluvial floodplain, where downward changes in resistivity in EF2 appears more gradational (excepting the resistive heterogeneities previously discussed), with the highest resistivity (100-110 ohm-m) values occurring near the top of EF2 and the lowest resistivities (20-25 ohm-m) occurring at the base, immediately above EF3 (e.g., Fig. 7b). The boundary between EF2 and EF3 separates conductive saturated alluvium from highly conductive fine-grained bedrock formations of the confining unit (the White River Group, which consists of the Brule and Chadron Formations and the underlying

Pierre Formation) at elevations ranging from 1055-1110 m.a.s.l. A moderate to sharp resistivity gradient generally denotes the bedrock surface, which is typically characterized by resistivities less than 20 ohm-m. Areas where the resistivity gradient is sharpest are interpreted to result from the presence of more clay/ash rich bedrock and/or higher pore-fluid content than in areas where the interface is characterized by more moderate resistivity gradients.

In a few profiles, the bedrock horizon exhibits weak resistivity gradients. These areas are typically associated with paleo-topographic lows (below approximately 1075 m.a.s.l.) and correspond to noticeably higher bedrock resistivity values (25-60 ohm-m). In a few areas the bedrock horizon is not well imaged (e.g., profiles 1 and 4 in Figs. 7a and 7d). Interpreted bedrock surfaces lacking a moderate to sharp resistivity gradient point to the removal of the Brule and Chadron Formations, as drilling logs indicate the presence of the massive Pierre Shale Formation immediately below EF2 at these locations. Characteristically, the Pierre Shale is comprised of layers with high clay content that contain bound water, resulting in a slightly more conductive unit than overlying formations of the White River Group [Anderson et al., 2009]. However, more electrically resistive lithologies commonly exist as heterogeneities within the upper part of the Pierre Shale, such as large limestone concretions and sandy beds partially cemented with calcium carbonate [Bjorkland and Brown, 1957]. Many test wells located within close proximity to the poorly resolved bedrock regions (approximately 4 km to the southwest and 8 km to the northeast) do not penetrate the Pierre Formation, but within the greater region of study (approximately 16 km to southwest and 22 km to the northeast) limestone layers and sandy sections have been identified in the bottom of wells. These features should have resistivities closer to that of the overlying alluvium which would result in a decreased resistivity gradient. Therefore we interpret the higher resistivity and corresponding weak resistivity gradient seen in portions of some of the profiles to result from the presence of these lithological heterogeneities existing within the upper part of the Pierre Shale. Profile 1 and profile 4 (Figs. 7a and 7d), provide examples, showing the surface of the confining unit as it transitions laterally from clay/ash rich formations of the White River Group to interpreted coarser grain layers of the underlying Pierre Shale. In profile 1 (Fig. 7a), low resistivities and a sharp vertical resistivity gradient are present at the top of EF3 at profile locations between 0-180 m. Resistivity in EF3 increases gradually between 180-390 m. At approximately 400 m, where the vertical resistivity gradient at the top of the facies begins to decrease we also observe a sharp horizontal resistivity gradient within EF3, marking the transitions from the low resistivity White River Group to a more electrically resistive lithology within the upper Pierre Shale.

The top of facies EF3 is interpreted to represent the bedrock surface, and exhibits substantial topographic relief (1055-1110 m.a.s.l.). For instance, an elongated stair step horizon is observed in profile 1 (Fig. 7a), decreasing in elevation to the southeast from approximately 1090 m.a.s.l. to 1068 m.a.s.l. In profile 2 (Fig. 7b), more frequent, opposing stair stepping forms emanate from a 40 m wide flat top paleo-topographic high (corresponding to 535-575 m). This feature is observed at approximately 1097 m.a.s.l., descending southwesterly to 1065 m.a.s.l. and northeasterly to 1073 m.a.s.l., respectively. The bedrock interface in profile 2 and 3 indicate a large-scale paleo-topographic depression in the center of the study area (Fig. 7b and 7c, respectively). Profile 5 also indicates a large-scale depression characterized by an undulating terrain consisting of short wavelength, 25-45 m wide, paleo-topographic highs and lows (Fig. 7e).

In order to interpret the confining bedrock surface three-dimensionally, a depth structure map was developed by contouring depths to the interpreted bedrock horizon measured at 10 m intervals along each profile, supplemented with bedrock depths from borehole data (Fig. 8). The majority of the surface lies on the northern bank of the previously recognized incised former river channel discussed in Section 2.2. The contour map reveals a highly variable terrain consisting of gently sloping areas, terraces, flat top buttes, ridges, gullies, gulches, narrow canyons, and large-scale paleo-topographic lows that has not been previously recognized. Only a portion of the southern bank of the channel is identified in the study area (southeastern region). The map shows a paleo-channel that is more deeply incised, has a stronger northeasterly trend, and a much narrower channel bottom (300-400 m compared to 600-1000 m) than described by Hurr et al. [1973a] (Fig. 5). The bottom of our mapped river channel occurs at similar depths as indicated by Hurr et al. [1973a] (corresponding to 1065 m.a.s.l.) but is differentiated by robust flat-topped buttes within the channel. These features are approximately 300 m wide and rise 15-20 m above the channel bottom (corresponding to elevations ranging from 1065-1085 m.a.s.l.) and are interpreted to represent erosional remnants of resistant Pierre Shale. To the north, the channel branches and narrowly extends 850 m to the northwest before significantly widening into a large-scale paleo-topographic low that trends southwest to northeast. This topographic low appears as a 35-40 m depression in the center of the map that corresponds to elevations ranging 1055-1095 m.a.s.l. with a maximum width of 700 m (observed in profiles 2 and 3, respectively in Figs. 7b and 7c). This feature describes an amphitheater shaped valley with an abrupt valley head wall and less steep sideslopes that is comprised of multiple narrow canyons with near vertical faces. A smaller southeast trending depression is incised into the valley floor that grades upslope and eventually merges with the paleo-channel. Near the north-central edge of the map a second large-scale paleo-topographic low is observed just above the box shaped valley and separated by a relatively flat plateau. This feature consists of a 20-25 m closed elongate depression that occurs at higher elevations ranging from 1085-1110 m.a.s.l. and has a maximum width of 700 m with a northeasterly trend. The closed depression corresponds to the undulating topography observed in profile 5 (Fig. 7e), describing adjacent narrow canyons with a segregated canyon floor and gully features that narrow to the northeast before disappearing into more level topography.

5. Discussion

The above results indicate eolian sand deposits do not readily store groundwater, but act as infiltration zones to underlying alluvial layers that comprise the primary aquifer storage unit that is underlain by fine-grained bedrock formations. Heterogeneities on the scale of 25-80 m within the uppermost part of the alluvium (EF2) and topography on the confining bedrock surface (EF3) potentially influence groundwater flow within the study area. The cause of these heterogeneities and the bedrock topography and their potential impact on groundwater flow are discussed below, once again beginning with the shallowest features and proceeding to the deepest.

The electrically conductive zone present in the upper alluvial layer beneath the eolian sand hills in the vicinity of the recharge ponds (at the top of EF2; Fig. 3) could result from locally increased clay fraction, more porous sediments, or a higher concentration of dissolved solids in the pore-fluids [Archie, 1942]. An electrically conductive pore fluid was initially suspected, due to the zones' proximity to artificial recharge operations. However, water-sampling indicates pumped groundwater located in the recharge ponds is chemically and electrically similar to the pore fluid within the eolian and alluvial layers [Beckman, 2007]. Hence, it is doubtful that the electrically conductive layer at the top of EF2 beneath the eolian sand in the areas near the recharge ponds is a result of highly conductive groundwater introduced through artificial recharge.

The lithological log near the recharge pond (Fig. 3) describes a 12 m section of clays and gravels with an upper 4.6 m clay layer corresponding to the top of the conductive zone, indicating a more abundant clay fraction in this area than is typical of the facies (Poceta, 2005). We therefore interpret the conductive zone to represent clay deposits similar to those described in the lithological log near the recharge pond (Fig. 3) rather than more porous sediments. ERT results indicate that these clay-rich strata form discontinuous lobate conductive bodies with variable spatial and depth distribution (Fig. 3). We speculate that clay layers exert a complex level of control on initial groundwater flow paths emanating from recharge ponds. The clay-rich electrically conductive zone in the upper part of the alluvial layer should have a relatively low hydraulic conductivity, effectively impeding the flow of water until enough hydraulic head develops to force the water downward into the deeper more transmissive part of the alluvial layer.

To better understand the nature of the bedrock surface at Tamarack, we compare our bedrock map to outcrop analogs of the Tertiary Brule Formation located 100 km due west of the study area at Pawnee Buttes National Grassland (Pawnee Buttes) near Grover, Colorado (location in Fig. 2). The confining bedrock surface map describes a rugged paleo-landscape comprised of unique erosional forms that strongly resemble bedrock exposures at Pawnee Buttes (Figs. 9a-f). The sculpted topography of Pawnee Buttes is comprised of numerous gullies and terraces that have progressed headward to develop distinctive, steeply sloping features [Henderson, 1907]. These form elongate topographic lows similar to those seen on the Tamarack bedrock structure map (Fig. 8). Erosional groundwater in the form of piping networks has largely shaped the Brule Formation into the irregular landscape present at Pawnee Buttes [Wohl et al., 2009]. We interpret the rugged paleo-topography imaged in the ERT data and shown in the bedrock structure map, featuring large-scale paleo-topographic lows carved into the confining bedrock surface, to result from similar groundwater outflow by piping and sapping. This interpretation is based on a) favorable bedrock lithologies, which are similar at Pawnee Buttes and within the Tamarack study area (involving the White River Group and underlying Pierre Shale); and b) the similarity in relief geometries (spacing between elevated features, horizontal scale of high and low relief features, vertical relief, and the morphology of headland, valley floor, and uplands), which have been attributed to piping networks at Pawnee Buttes [Wohl et al., 2009]. In the southern part of the study area, we interpret the bedrock morphology to be dominated by fluvial incision and formation of a broad (300-400 m wide) and deep (1065 m.a.s.l.) paleo-river valley, as previously suggested by Hurr et al. [1973a].

The northernmost paleo-topographic low shown on the bedrock map is 700 m wide and 20-25 m deep, corresponding to elevations 1085-1110 m.a.s.l. (Feature A in Fig. 8). This paleo-valley is characterized by a closed depression with narrow gully features that is interpreted to largely result from groundwater piping. Extensive piping networks readily develop within sediments similar to the White River Group, such as loosely cemented siltstones and claystones that contain swelling clay minerals and form desiccation cracks in dry conditions [Parker, 1963]. The piping process is initiated above the groundwater table as surface waters flow downward through fractures, desiccation cracks, and other openings. These descending waters eventually encounter the water table or an impermeable layer that laterally drives groundwater through an outflowing point of weakness [Higgins, 1984]. An example is shown in Fig. 9c, showing outflowing pipes present in fractured Brule Formation outcrops with heterogeneous pebble deposits at Pawnee Buttes. Progressive enlargement of these internally weak zones results in collapse structures that can create extensive gully networks and pseudokarst features [Higgins, 1984] as well as triggering landslides, bank failures, and the development of badlands [Jones, 1994]. High swelling clay contents within the Chadron and Pierre Formations have been suggested to have led to the formation of pseudokarst terrains that form closed depressions and other karst-like features at Badlands National Park [Graham, 2008]. The closed paleo-depression identified within the study area (700 m wide, 20-25 m deep; at elevations 1085-1110 m.a.s.l. in Fig. 8) is similar to the pseudokarst terrains described above that have been attributed to the collapse of piping networks [Harris et al., 2003]. The presence of small-scale gully features at the northeastern end of the paleo-depression suggests piping failure initially formed gully networks before coalescing into a larger closed gulch structure through ensuing mass movements. Eolian transport gradually removed slumped material from the depression and much greater volumes of sediment were carried away during storm events [Henderson, 1907].

Conversely, the more deeply-incised paleo-topographic low observed in the center of our bedrock map (700 m wide, 35-40 m deep; at elevations 1055-1095 m.a.s.l. in Fig. 8) consists of an amphitheater shaped valley that is interpreted to have formed largely by groundwater sapping processes. Sapping occurs below the water table, where groundwater emerges as concentrated outflow at seepage or spring sites and leads to the undermining and collapsing of channel heads and sidewalls [Laity and Malin, 1985]. Sapping typically initiates in zones of structural weakness that increase permeability, such as heavily fractured bedrock, localized lithologic heterogeneities, and other areas highly susceptible to piping [Dune, 1980; Kochel et al., 1985]. Concentrated groundwater outflow, aided by well-connected pipe networks through structurally weakened zones contributes to the headward advance of channels and valleys that can create large-scale drainage systems [Higgins, 1984]. Sapping landforms characteristically describe near vertical amphitheater channel heads with steep sidewalls, a U-shaped cross section, and a flat floor [Luo, 2000].

The deep paleo-topographic low at Tamarack (700 m wide, 35-40 m deep; at elevations 1055-1095 m.a.s.l.; Feature B in Fig. 8) is interpreted to have resulted from an extensive sapping network that formed within the paleo-channel and progressed headwards to the northwest. We suggest headward erosion resulted preferentially through fractured bedrock that may have been further weakened by piping networks. Therefore, the observed channel progression corresponds to the increased potential for groundwater sapping to exist in deeply incised channels and in formations where water flows through fractures and desiccation cracks [Pederson, 2001]. The sapping network displays distinctive amphitheater valley head morphology that rises abruptly from the valley floor (Fig. 8). The incised depressions on the valley floor are attributed to surface runoff and the less steep sideslopes signify a relict valley whose sidewalls have been graded by rilling and mass wasting [Higgins, 1984]. The infilling of alluvium during the Pleistocene likely halted the headward advancement of the valley head, effectively transitioning groundwater outflow at sapping sites to groundwater flow through the recently deposited alluvial sediments.

Bedrock features comprising the buried paleo-landscape at Tamarack potentially act as preferential flow pathways for recharging waters. The deeply incised amphitheater head valley (700 m wide, 35-40 m deep; at elevations 1055-1095 m.a.s.l.; Feature B in Fig. 8) interpreted to result from sapping processes possibly redirects flow away from the river, limiting groundwater flow into the river channel from the artificial recharge area located in the eolian hills approximately 1 km south of the river. The complex bedrock topography establishes a previously unrecognized first order control on groundwater flowpaths within the unconfined alluvial aquifer. Heavily eroded landforms resulting from groundwater outflow processes potentially span across the South Platte alluvial aquifer and High Plains aquifer in regions confined by the Tertiary White River Group (Fig. 2).

6. Conclusions

ERT integrated with well data and laboratory resistivity measurements has proven an effective approach in developing hydrogeologic models of alluvial aquifer systems underlain by electrically conductive sedimentary formations. Local geology corresponds to 3 electrostratigraphic units that have been correlated with drilling logs and laboratory resistivity measurements to develop a hydrostratigraphic model and confining bedrock surface map. Results indicate eolian sand deposits (50-800 ohm-m) are largely unsaturated and do not readily store groundwater but serve as infiltration zones. The underlying alluvium (20-3890 ohm-m) functions as the primary groundwater storage unit and exhibits highly variable resistivities corresponding to heterogeneous alluvial layers and groundwater withdrawal. Resistive anomalies are observed near pumping wells in the alluvial floodplain and correlate to a total area of pumping induced drawdown that intercepts the South Platte River. An intermittent conductive zone (25-80 ohm-m) comprised of lobate bodies occurs beneath the sand hills and is attributed to clay deposits of varying scale. A localized concentration of interspersed clays within the upper alluvium has the potential to influence initial groundwater flow paths of recharging waters. Groundwater flow may also be influenced by complex erosional forms found to exist on the surface of highly conductive fine-grain bedrock formations (1-60 ohm-m) that confine the aquifer system. The bedrock surface is most prominently characterized by large-scale paleo-topographic lows (700 m wide, 35-40 m deep; 700 m wide, 20-25 m deep) that occur on the northern bank of a previously recognized incised paleo-channel. These features are largely carved into formations of the White River Group and are interpreted to result from groundwater outflow processes (piping and sapping), which have heavily eroded White River outcrops within the northern Great Plains. The rugged bedrock topography establishes a previously unrecognized first order control on groundwater flowpaths within the unconfined South Platte alluvial aquifer and extensive erosion via groundwater piping and sapping processes may characterize the bedrock configuration underlying portions of the High Plains aquifer.

7. Recommendations

Further investigation and data acquisition are required to understand the complex hydrogeologic system at Tamarack. Recommendations for future projects that could shed light on subsurface groundwater controls at Tamarack, as well as suggestions to improve surveying and enhance data quality include:

1. ERT results indicate clay-rich strata form lobate conductive bodies with variable spatial and depth distribution beneath artificial recharge areas. The presence of increased clays near the top of the alluvial layer may have profound implications on groundwater flow returning to the river and should be further studied. This investigation has outlined the approximate areal extent of these interpreted features that can be utilized to develop a more a detailed ERT survey within the area (Fig. 3). A pilot study should be conducted around well T-13 to delineate the spatial dimensions of the clay layers indicated in the lithological log and determine suitable electrode spacing for imaging ~1-5 m thick clays that are 10-40 m beneath the surface. It would be interesting to collect data during the fall and spring (at times when the ground is moist to increase data quality) in order to also assess changes in the water-table corresponding to the pumping cycle and the formation and extent of groundwater mounds below recharge areas that potentially correlate to the distribution of clay deposits.

2. The features identified on the bedrock surface in this study need to be further resolved through supplemental geophysical surveying. This study has shown ERT is able to readily distinguish highly conductive bedrock regions of the White River Group and Pierre Shale using a dipole-dipole array and 10 m electrode spacing. However, more resistive regions appearing at greater depths (below 1075 m.a.s.l.), attributed to heterogeneities in the Pierre Shale, are not as easily identified by ERT. An extensive seismic refraction survey should be conducted to better resolve these regions and to support findings presented in this thesis. In order to collect interpretable data, seismic surveying needs to be conducted at times when groundwater pumps are shut off and noise pollution can be limited. Surveying during colder months at times when the ground is hard will likely produce the best results.

8. Figures

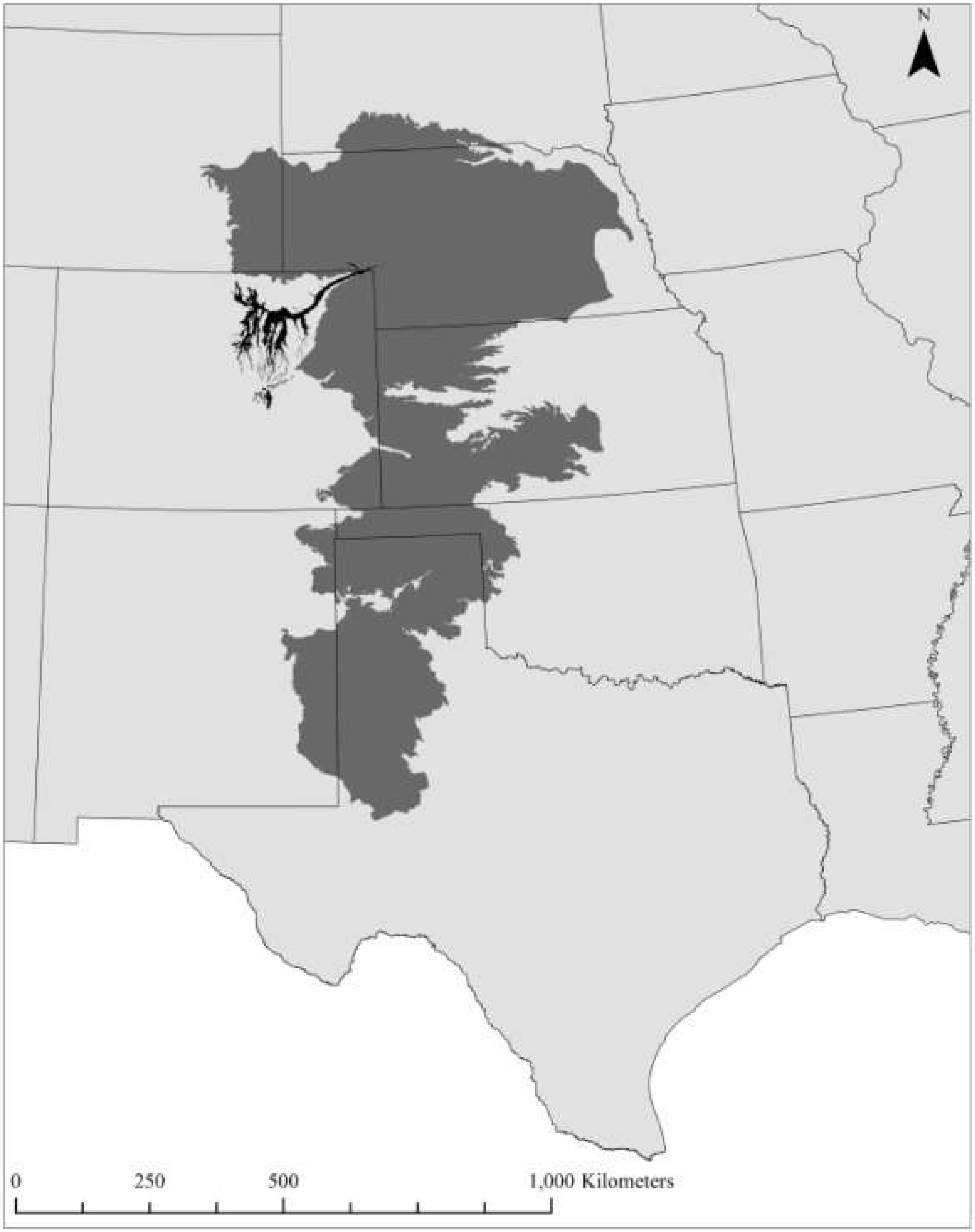

Figure 1: Location of the High Plains aquifer (grey) and South Platte River alluvial aquifer (black) of the North American Great Plains. Adapted from Qi [2009]

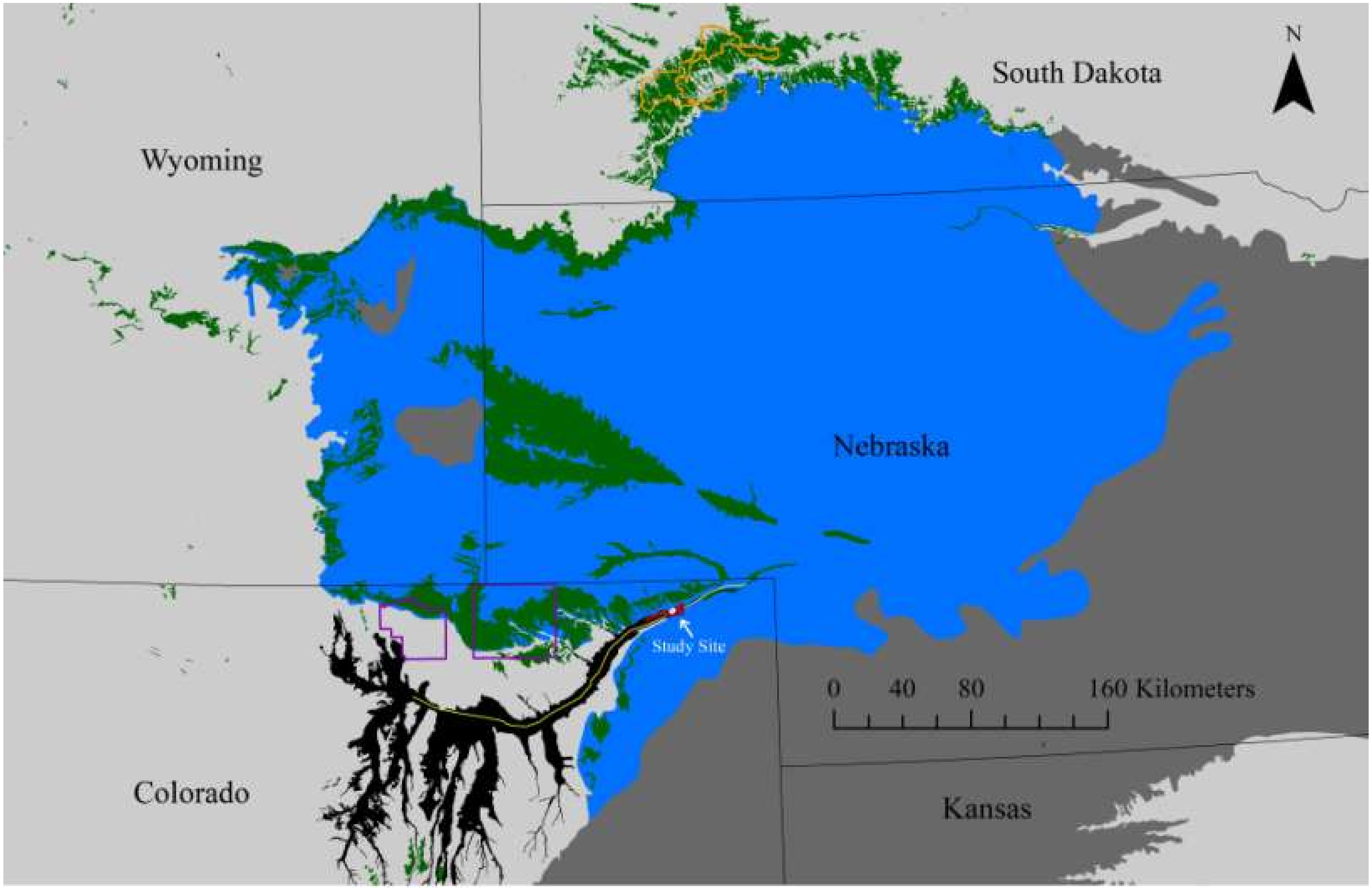

Figure 2 Distribution of hydrostratigraphic units in the Lower South Platte River Valley and adjacent areas. The Tertiary White River Group serves as the confining aquifer unit (blue) for 28% of the High Plains aquifer (grey) [Weeks and Gutentag, 1981] and a portion of the South Platte alluvial aquifer (black). Trace of paleo-channel (yellow line) identified by Hurr et al. [1972; 1973a, 1973b, 1973c, and 1973d]. Outcrops of the White River Group (green) are scattered across the northern Great Plains. Study site (white dot indicated by arrow) is within the Tamarack Ranch State Wildlife Area (red). At Pawnee Buttes (purple) and Badlands National Park (orange) there are surface exposures of landforms that provide analogs to features discussed in the text. Adapted from Qi [1999]; Stoeser et al. [2005]; Qi [2009]

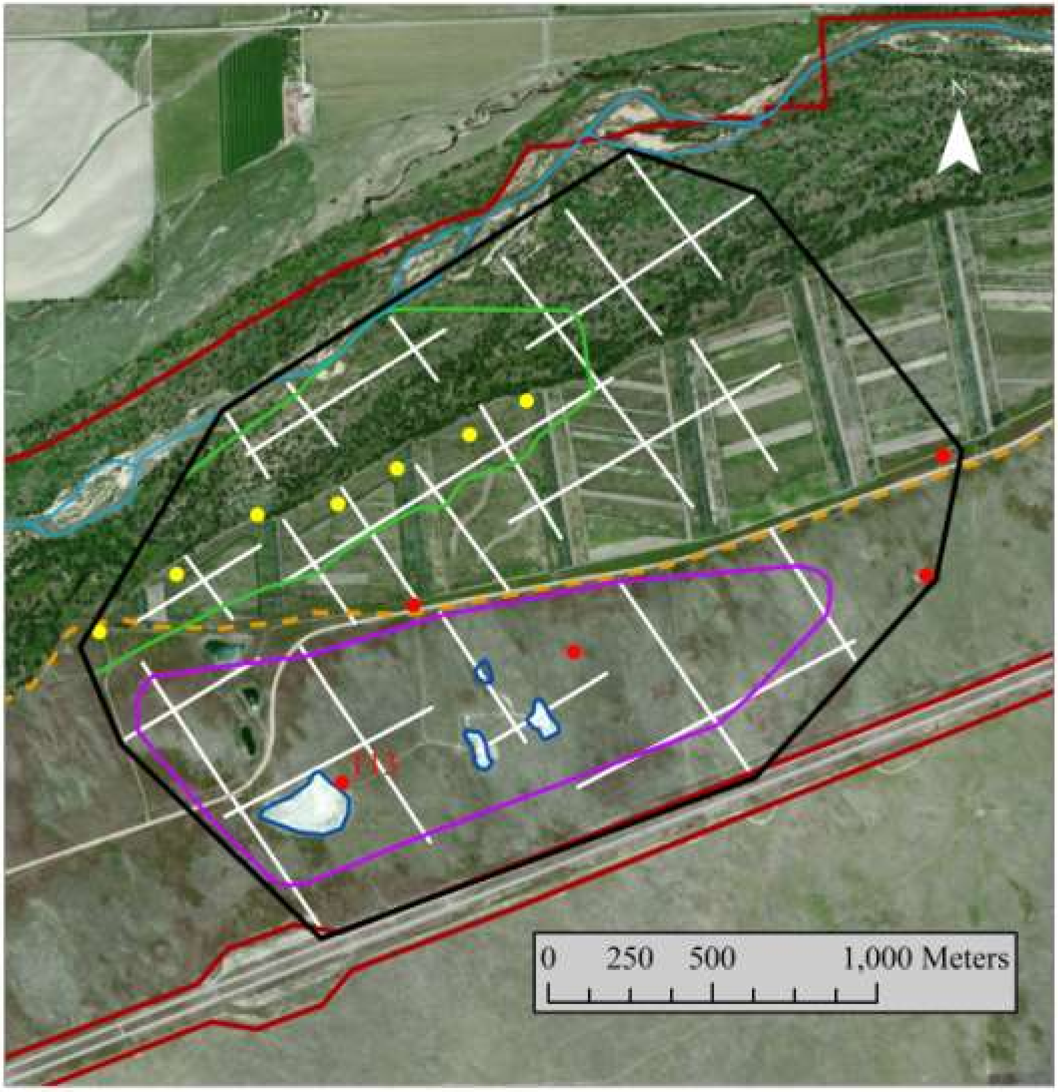

Figure 3: Study site (outlined in black) located at Tamarack Ranch State Wildlife Area (outlined in red) is situated on the floodplain of the braided South Platte River (blue) and adjacent eolian sand hills (orange dashed line denotes surface contact between exposed alluvial sediments to the north and surficial eolian sediments to the south). Groundwater is extracted from the aquifer near the South Platte River (yellow circles denote pumping wells) and pumped to recharge ponds that are outlined in dark blue situated in upland eolian sand deposits. The ERT survey included twenty-seven DC electrical resistivity profiles (white). Borehole data (yellow and red circles) within the study area was integrated with ERT data to constrain bedrock configuration as discussed in the text. ERT data indicates pumping induced drawdown in the area outlined in green. Purple line shows extent of discontinuous clay deposits encountered within the upper part of the alluvial layer in borehole T13 (adjacent to the main recharge pond) that is inferred from the ERT data.

<table>
<tr><th>System</th><th colspan="2">Stratigraphy</th><th>Hydrologic Function</th><th>Electrostratigraphy</th></tr>
<tr><td rowspan="2">Quaternary</td><td colspan="2">Eolian Sand</td><td>Infiltration Unit</td><td>Electro-facies 1
(50-800 ohm-m)</td></tr>
<tr><td colspan="2">Alluvium</td><td>Aquifer Unit</td><td>Electro-facies 2
(25-3890 ohm-m)</td></tr>
<tr><td rowspan="2">Tertiary</td><td rowspan="2">White River Group</td><td>Brule Formation</td><td rowspan="3">Confining Unit</td><td rowspan="3">Electro-facies 3
(1-60 ohm-m)</td></tr>
<tr><td>Chadron Formation</td></tr>
<tr><td>Cretaceous</td><td colspan="2">Pierre Formation</td></tr>
</table>

Figure 4: Stratigraphic nomenclature at Tamarack Ranch State Wildlife Area, near Crook, CO follows Bjorkland and Brown [1957] and correlates with electrostratigraphy observed in ERT data.

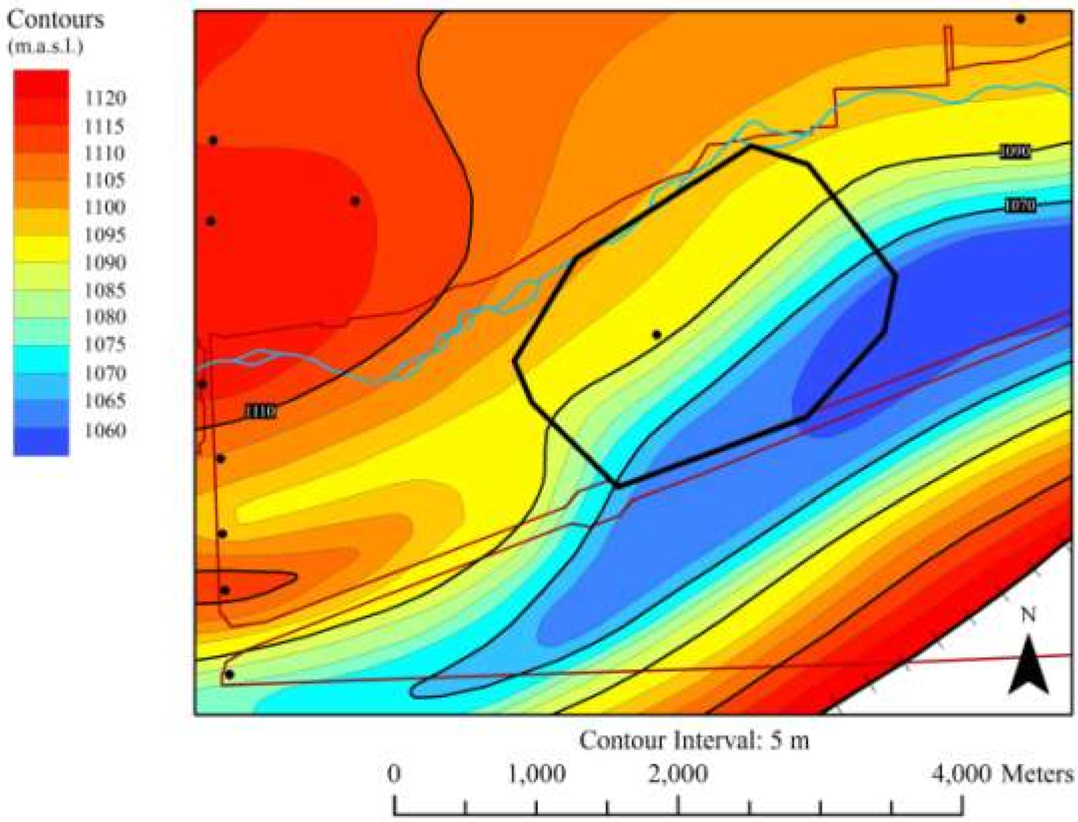

Figure 5: Bedrock structure contour map constrained by borehole data (black circles) within the vicinity of study area (modified from Hurr et al. [1973a]). Black outline shows region where new geophysical data was collected to create map shown in Fig. 8. Hatched line indicates southern extent of bedrock map. Tamarack Ranch State Wildlife Area boundaries are shown in red, braided South Platte River channel traces in blue. Contours are labeled in meters above sea level. Thick black line marks 20 m change in elevation.

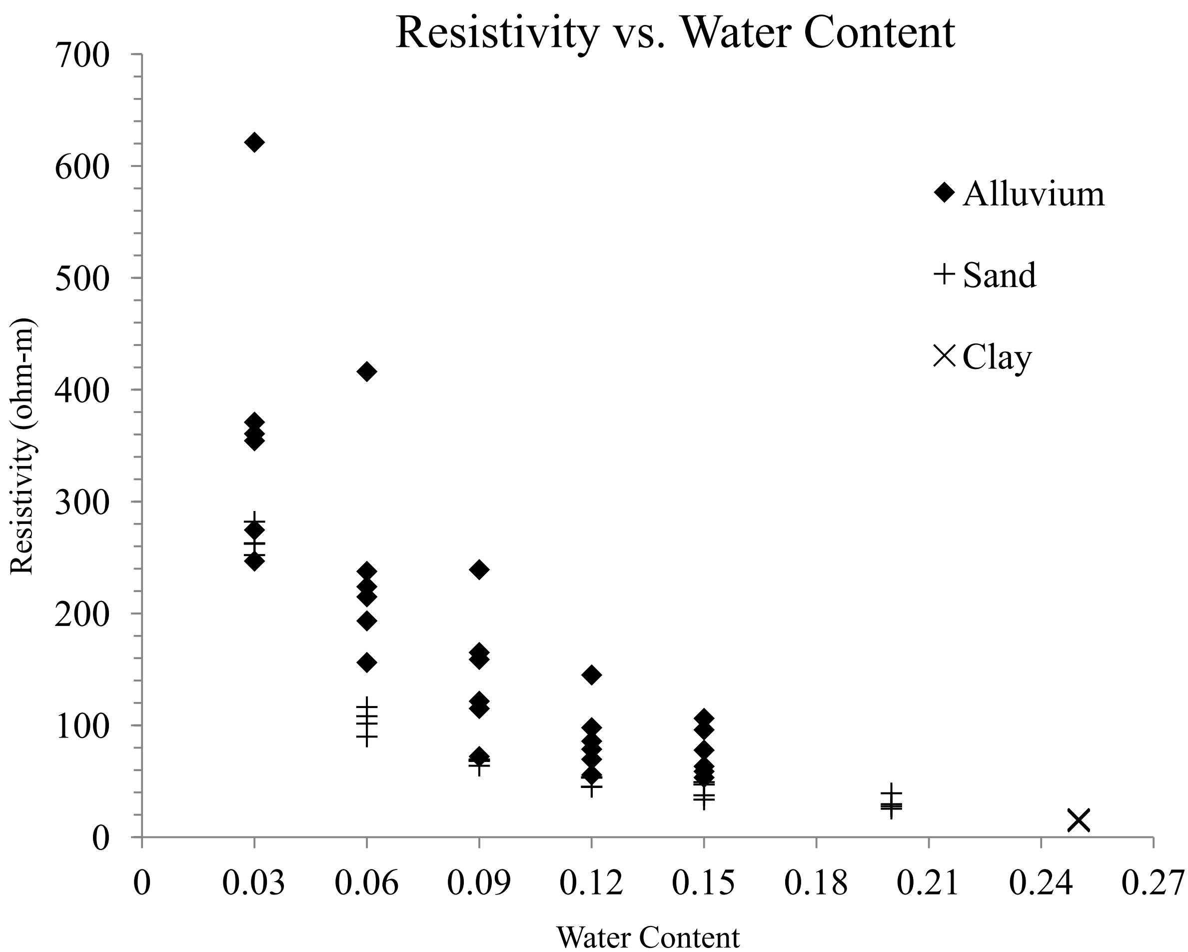

Figure 6: Laboratory resistivity measurements for representative lithologies present at the study site. Alluvium: black diamonds; eolian sands: black plus symbol; clays: black cross symbol.

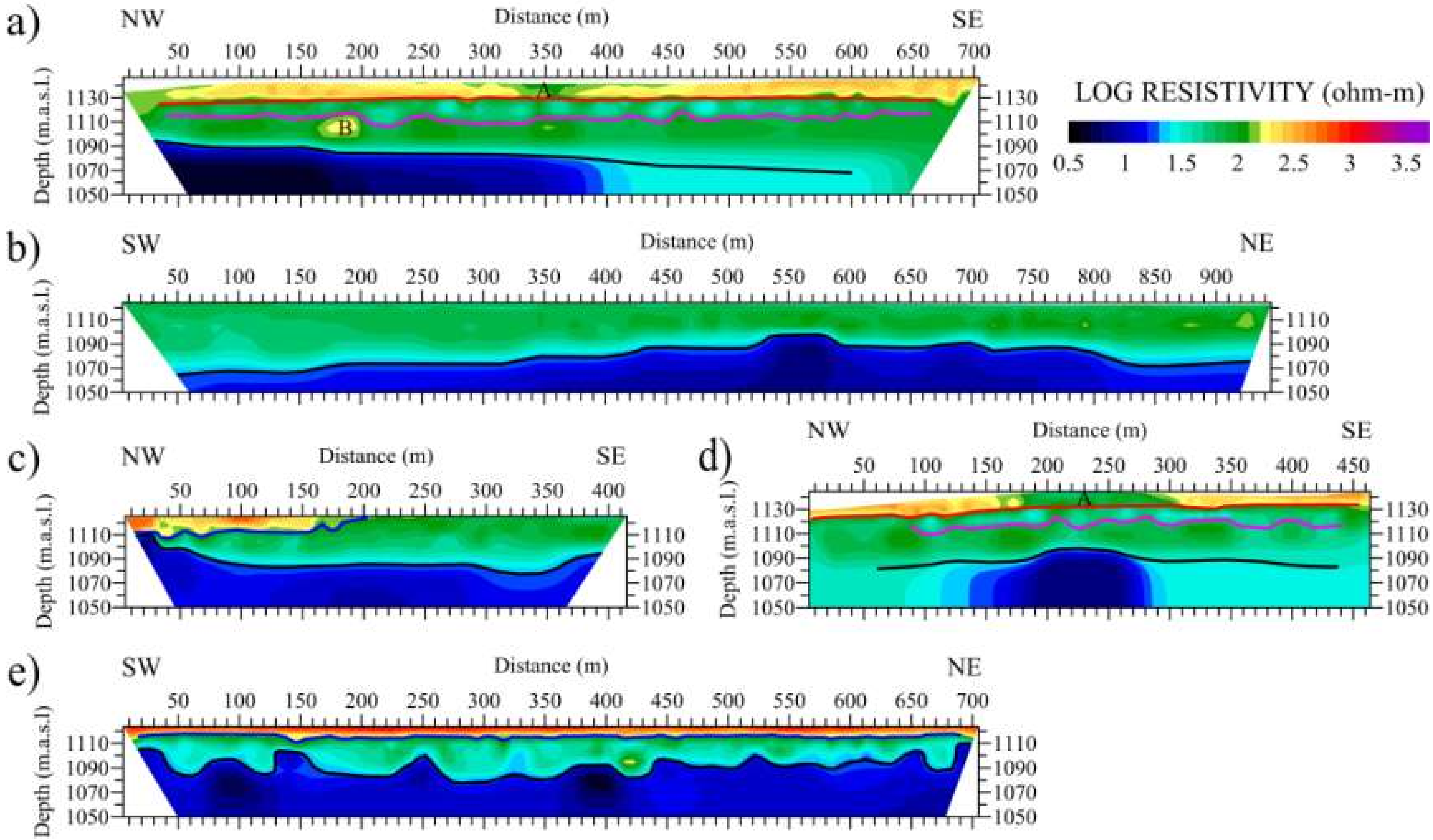

Figure 7: Inverted resistivity data: a) profile 1; b) profile 2; c) profile; d) profile 4; e) profile 5. Upper red line denotes water table and boundary between eolian sands (EF1) and underlying saturated alluvium (EF2), lower black line denotes boundary between saturated alluvium (EF2) and underlying bedrock (EF3). Upper blue line denotes maximum depth of resistive anomaly correlated to pumping induced drawdown, purple line denotes maximum depth of conductive zone within upper alluvial layers correlating to clay layers and upper case letters denote heterogeneities within electro-facies, see discussion in text.

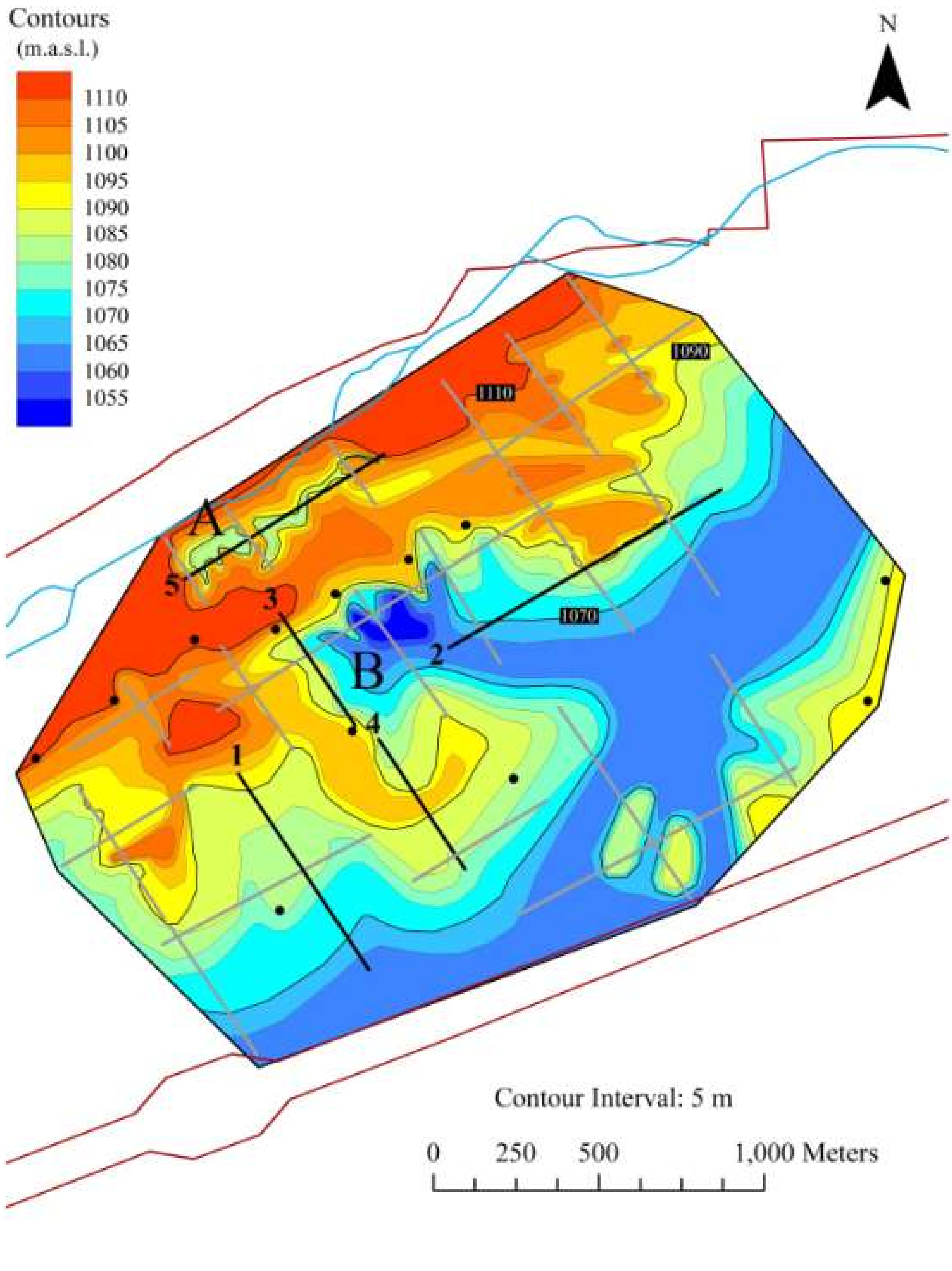

Figure 8: Bedrock surface map, developed from 2D interpreted bedrock profiles (grey and black lines) and bedrock depths from borehole data (black circles). Tamarack Ranch State Wildlife Area boundaries are shown in red, braided South Platte River channel traces in blue. Contours are labeled in meters above sea level. Thick black line marks 20 m change in elevation. Numbers indicate profiles and upper case letters indicate features discussed in this paper.

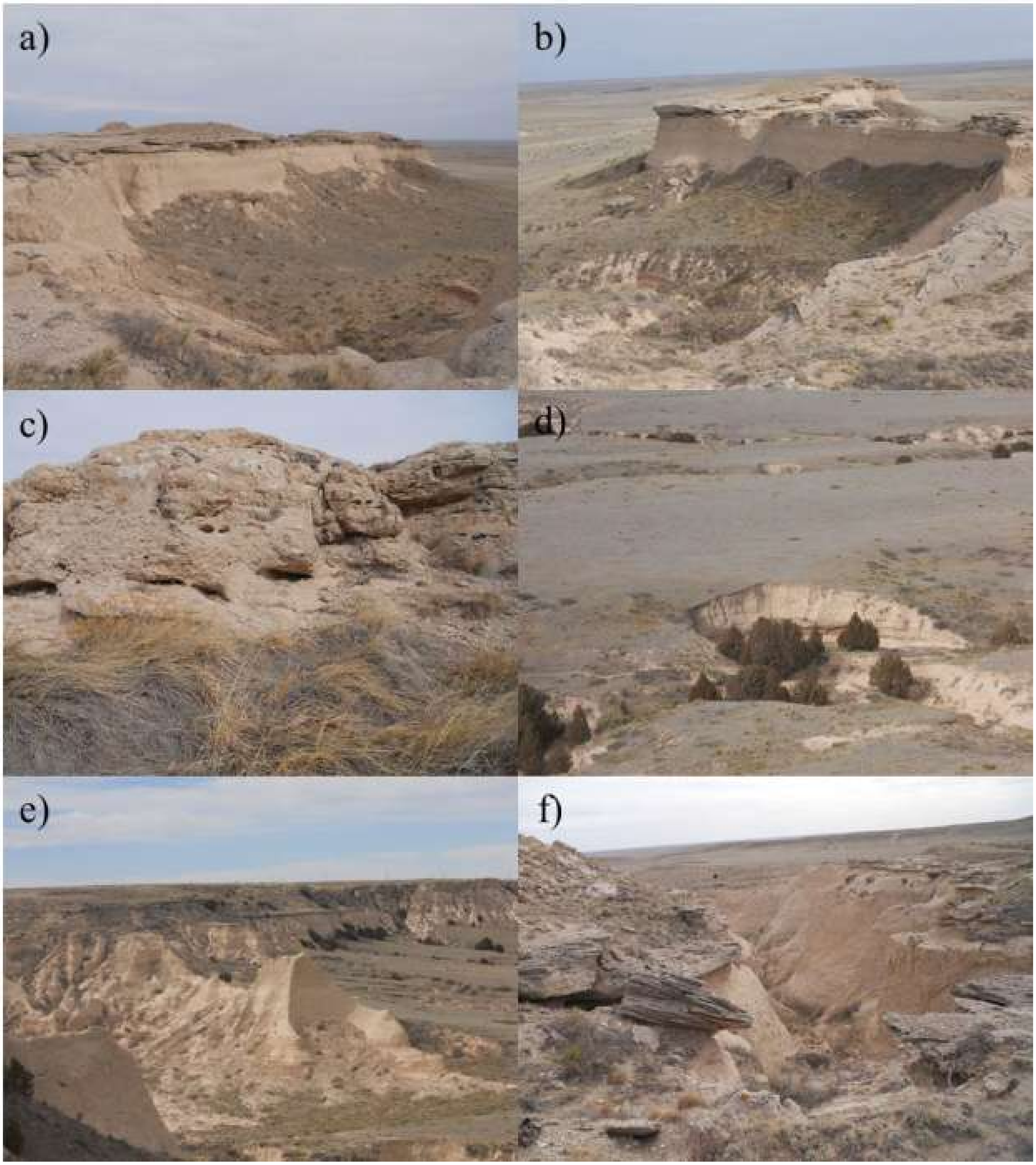

Figure 9: Outcrop analogs, Brule Formation capped by thin veneer of sandstone in areas; Pawnee Buttes National Grasslands, Grover, CO: a) steep headcut; b) steep head cut with depression on valley floor; c) evidence of piping networks in fractured Brule Formation with heterogeneous pebble deposits; d) closed depression; e) narrow topographic high; f) narrow canyon

9. References

Anderson, J.A., R.H. Morin, J.C. Cannia, and J.H. Williams (2009), Geophysical Log Analysis of Selected Test Holes and Wells in the High Plains Aquifer, Central Platte River Basin, Nebraska, *Scientific Investigations Report 2009-5033*, U.S. Geol. Surv., Reston, Virginia, United States.

Archie, G.E. (1942), The electrical resistivity log as an aid in determining some reservoir characteristics, *Transactions, American Institute of Mining, Metallurgical and Petroleum Engineers*, 146, 54-62.

Barber, N.L. (2009), Summary of estimated water use in the United States in 2005, *Factsheet 2009-3098,* U.S. Geol. Surv., Reston, Virginia, United States.

Barrash, W., and R.H. Morin (1987), Hydrostratigraphy and distribution of secondary permeability in the Brule Formation, Cheyenne County, Nebraska, *Geological Society of America Bulletin,*99, 445-462.

Beckman, N.A. (2007), Quantifying groundwater and surface water mixing at a conjunctive use site, M.S. thesis, pp 180, Colorado State University, Fort Collins, Colorado, United States.

Bjorklund, L.J., and R.F. Brown (1957), Geology and Ground-Water Resources of the Lower South Platte River Valley Between Hardin Colorado, and Paxton Nebraska, *Water-Supply Pap. 1378*, U.S. Geol. Surv., Washington, D.C.

Bouwer, H. (2002), Artificial recharge of groundwater: hydrogeology and engineering, *Hydrogeology Journal*, 10, 121-142, doi: 10.1007/s10040-001-0182-4.

Bredehoeft, J (2011), Hydrologic Trade-offs in Conjunctive Use Management, *Groundwater*, 9(4), 468-475, DOI: 10.1111/j.1745-6584.2010.00762.x

Condon, S.M. (2005), Geologic studies of the Platte River, South-Central Nebraska and adjacent areas-Geologic maps, subsurface study, and geologic history, *Professional Paper 1706*, U.S. Geol. Surv., Reston, Virginia, United States.

Dahlin, T., and B. Zhou (2004), A numerical comparison of 2D resistivity imaging with 10 electrode arrays, *Geophysical Prospecting*, 52, 379-398.

Dunne, T. (1980), Formation and controls on channel networks, *Progress in Physical Geography*, 4, 211-239.

Gesch, D.B. (2007), The National Elevation Dataset: Digital Elevation Model Technologies and Applications, in *The DEM User's Manual*, 2nd ed., edited by D.F. Maune, pp. 99-118, American Society for Photogrammetry and Remote Sensing, Bethesda, Maryland, United States.

Graham, J. (2008), Badlands National Park Geologic Resource Evaluation Report, *Natural Resource Report NPS/NRPC/GRD/NRR-2008/036,* National Park Service, Denver, Colorado, United States.

Harris, A.G., E. Tuttle, and S.D. Tuttle (2003), Geology of National Parks, Sixth ed., Kendall Hunt Publishing Company, Dubuque, Iowa, USA.

Henderson J. (1907), Topographic Development of Chalk Bluffs and Pawnee Buttes, Proceeding of the Colorado Scientific Society, Vol. 8, 247-256.

Higgins, C.G. (1984), Piping and sapping: development of landforms by groundwater outflow, in *Groundwater as a geomorphic agent,* edited by R.G. La Fleur, pp. 18-58, Allen and Unwin, Boston, Massachusetts, United States.

Hurr, R.T., P.A. Schneider, and W.E. Hofestra (1972), Hydrogeologic characteristics of the valley-fill aquifer in the Greeley Reach of the South Platte River valley, CO., *Open-File Report 73-123-Plate 2*, Water Resources Division, U.S. Geological Surv., Lakewood, Colorado, United States.

Hurr, R.T., P.A. Schneider, and W.E. Hofestra (1973a), Hydrogeologic characteristics of the valley-fill aquifer in the Julesburg Reach of the South Platte River valley, CO., *Open-File Report 73-124-Plate 2*, Water Resources Division, U.S. Geological Surv., Lakewood, Colorado, United States.

Hurr, R.T., P.A. Schneider, and W.E. Hofestra (1973b), Hydrogeologic characteristics of the valley-fill aquifer in the Greeley Reach of the South Platte River valley, CO., *Open-File Report 73-125-Plate 2*, Water Resources Division, U.S. Geological Surv., Lakewood, Colorado, United States.

Hurr, R.T., P.A. Schneider, and W.E. Hofestra (1973c), Hydrogeologic characteristics of the valley-fill aquifer in the Sterling Reach of the South Platte River valley, CO., *Open-File Report 73-126-Plate 2*, Water Resources Division, U.S. Geological Surv., Lakewood, Colorado, United States.

Hurr, R.T., P.A. Schneider, and W.E. Hofestra (1973d), Hydrogeologic characteristics of the valley-fill aquifer in the Weldona Reach of the South Platte River valley, CO., *Open-File Report 73-127-Plate 2*, Water Resources Division, U.S. Geological Surv., Lakewood, Colorado, United States.

Jones, J.A.A. (1994), Soil piping and its hydrogeomorphic function, *Cuaternario Geomofol*., 8, 77-102.

Kochel, R.C., A.D. Howard, and C.F. McLane (1985), Channel networks developed by groundwater sapping in fine-grained sediments: analogs to some martian valleys, in *Models of Geomorphology*, edited by M.J. Woldenburg, pp. 313-341, Allen and Unwin, Boston, Massachusetts, United States.

Laity, J.E., and M.C. Malin (1985), Sapping processes and the development of theater-headed valley networks on the Colorado Plateau, *Geological Society of America Bulletin*, 96, 203-217.

Larson, E.E., and E. Evanoff (1998), Tephrostratigraphy and source of the tuffs of the White River sequence, in *Depositional Environments, Lithostratigraphy, and Biostratigraphy of the White River and Arikaree Groups: Geological Society of America Special Paper 325: (Late Eocene to Early Miocene, North America),* edited by D.O. Terry, H.E. LaGarry, and R.M. Hunt, pp. 1-14, Geological Society of America, Boulder, Colorado, United States.

Loke, M.H., and R.D. Barker (1996), Practical techniques for 3D resistivity surveys and data inversion, *Geophysical Prospecting*, 44, 499-523.

Loke, M.H, and T. Dahlin (2002), A comparison of the Gauss-Newton and quasi-Newton methods in resistivity imaging inversion, *Journal of Applied Geophysics*, 49, 149-162.

Loke, M.H., I. Acworth, and T. Dahlin (2003), A comparison of smooth and blocky inversion methods in 2D electrical imaging surveys, *Exploration Geophysics*, 34, 182-187.

Lucius, J.E., W.H Langer, and K.J. Ellefsen (2007), An introduction to using surface geophysics to characterize sand and gravel deposits, *Circular 1310*, U.S. Geol. Surv., Reston, Virginia, United States.

Luo, W. (2000), Quantifying groundwater-sapping landforms with a hypsometric technique, *Journal of Geophysical Research*, 105(E1), 1685-1694.

Maupin, M.A., and N.L. Barber (2005), Estimated Withdrawals from Principal Aquifers in the United States, 2000, *Circular 1279*, U.S. Geol. Surv., Reston, Virginia, United States.

McGuire, V.L. (2013), Water-level and storage changes in the High Plains aquifer, predevelopment to 2011 and 2009-11, *U.S. Geological Survey Scientific Report 2012-5291*, U.S. Geol. Surv., Reston, Virginia, United States.

Oldenburg, D.W., and Y. Li. (1999), Estimating depth of investigation in DC resistivity and IP Surveys, *Geophysics*, *64*, 403-416.

Parker, G.G. (1963), Piping, a geomorphic agent in landform development of the drylands, *International Association of Scientific Hydrology Publication No. 65*, 103–113.

Pederson, D.T. (2001), Stream Piracy Revisited: A Groundwater Sapping Solution, *GSA Today*, 11, 4-10.

Poceta, J.A. (2005), Electrical resistivity imaging of eolian and alluvial sediments along the south platte river, northeastern Colorado, M.S. thesis, pp 58, Colorado State University, Fort Collins, Colorado, United States.

Qi, S.L. (1999), This geospatial data set consists of the bedrock formations of the High Plains aquifer, which underlies parts of Colorado, Kansas, Nebraska, New Mexico, Oklahoma, South Dakota, Texas, and Wyoming, Version 1, March 2013 to May 2013, http://water.usgs.gov/GIS/metadata/usgswrd/XML/ofr99-214_hpbedrock.xml, Water Resources of the United States, U.S. Geol. Surv., Reston, Virginia, United States.

Qi, S.L. (2009), Digital map of aquifer boundary for the High Plains aquifer in parts of Colorado, Kansas, Nebraska, New Mexico, Oklahoma, South Dakota, Texas, and Wyoming, http://water.usgs.gov/GIS/metadata/usgswrd/XML/ds543.xml, Water Resources of the United States, U.S. Geol. Surv., Reston, Virginia, United States.

Reynolds, J.M (1997), An Introduction to Applied and Environmental Geophysics, John Wiley & Sons Ltd, Baffins Lane, Chichester, England.

Samadder, R.K., S. Kumar, and R.P. Gupta (2007), Conjunctive use of well-log and remote sensing data for interpreting shallow aquifer geometry in Ganga Plains, *Journal of the Geological Society of India*, 69, 925-932.

Samadder, R.K., S. Kumar, and R.P. Gupta (2011), Paleochannels and their potential for artificial groundwater recharge in the western Ganga plains, *Journal of Hydrology*, 400, 154-164.

Srivastava, A. (2005), Aquifer geometry, basement-topography and groundwater quality around Ken Graben, India, *Journal of Spatial Hydrology*, 2(2), 1-7.

Stoeser, D.B., G.N. Green, L.C. Morath, W.D. Heran, A.B. Wilson, D.W. Moore, and B.S. Van Gosen (2005), Preliminary integrated geologic map database for the United States: Central States: Montana, Wyoming, Colorado, New Mexico, North Dakota, South Dakota, Nebraska, Kansas, Oklahoma, Texas, Iowa, Missouri, Arkansas, and Louisana, Version 1.2, March 2013 to May 2013, http://pubs.usgs.gov/of/2005/1351/, Mineral Resource Program, U.S. Geol. Surv., Reston, Virginia, United States. (Updated 2007).

Tait, N.G., R.M. Davison, J.J. Whittaker, S.A. Lehame, and D.N. Lerner (2004), Borehole optimization system (BOS) – a GIS based risk analysis tool for optimizing the use of urban groundwater, *Environmental Modeling and Software*, 19, 1111-1124.

Telford, W. M., L. P. Geldart, and R. E. Sheriff (1990), Applied Geophysics, Second ed., Cambridge University Press, New York, New York, United States.

Terry, D.O. (1998), Lithostratigraphic revision and correlation of the lower part of the White River Group: South Dakota to Nebraska, in *Depositional Environments, Lithostratigraphy, and Biostratigraphy of the White River and Arikaree Groups: Geological Society of America Special Paper 325: (Late Eocene to Early Miocene, North America),* edited by D.O. Terry, H.E. LaGarry, and R.M. Hunt, pp. 15-39, Geological Society of America, Boulder, Colorado, United States.

Waltz, J.P. (1972), Geohydraulics at the unconformity between bedrock and alluvial aquifers, *Completion Rep. 30*, Colo. Water Resour. Res. Inst., Fort Collins, Colorado, United States.

Warner, J.W., J. Altenhofen, J. Odor, and B. Welch (1994), Recharge as augmentation in the South Platte River basin, *Groundwater Program Tech. Rep. 21*, Colo. Water Resour. Res. Inst., Fort Collins, Colorado, United States.

Weeks, J.B., and E.D. Gutentag (1981), Bedrock geology, altitude of base, and 1980 saturated thickness of the high plains aquifer in parts of Colorado, Kansas, Nebraska, New Mexico, Oklahoma, South Dakota, Texas, and Wyoming,

Wohl, E., S. Egenhoff, and K. Larkin (2009), Vanishing riverscapes: A review of historical channel change on the western Great Plains, in *Management and Restoration of Fluvial Systems with Broad Historical Changes and Human Impacts: Geological Society of America Special Paper 451*, edited by L.A. James, S.L. Rathburn, and G.R. Whittecar, pp. 131-142, Geological Society of America, Boulder, Colorado, United States.

10. Appendix

The data in this section is intended for archival purposes and includes: 1) bedrock map indicating locations for 27 ERT profiles; 2) the 27 ERT profiles that comprise the bedrock map; and 3) laboratory resistivity measurements for the alluvial, eolian, and clay samples. Also, data that has been digitally achieved includes: processing information and interpretations for each ERT profile as they correspond to the map provided below and figures presented in this thesis; 2) Arcgis databases used to interpret the bedrock surface; and 3) Arcgis files that contain figures presented in this thesis.

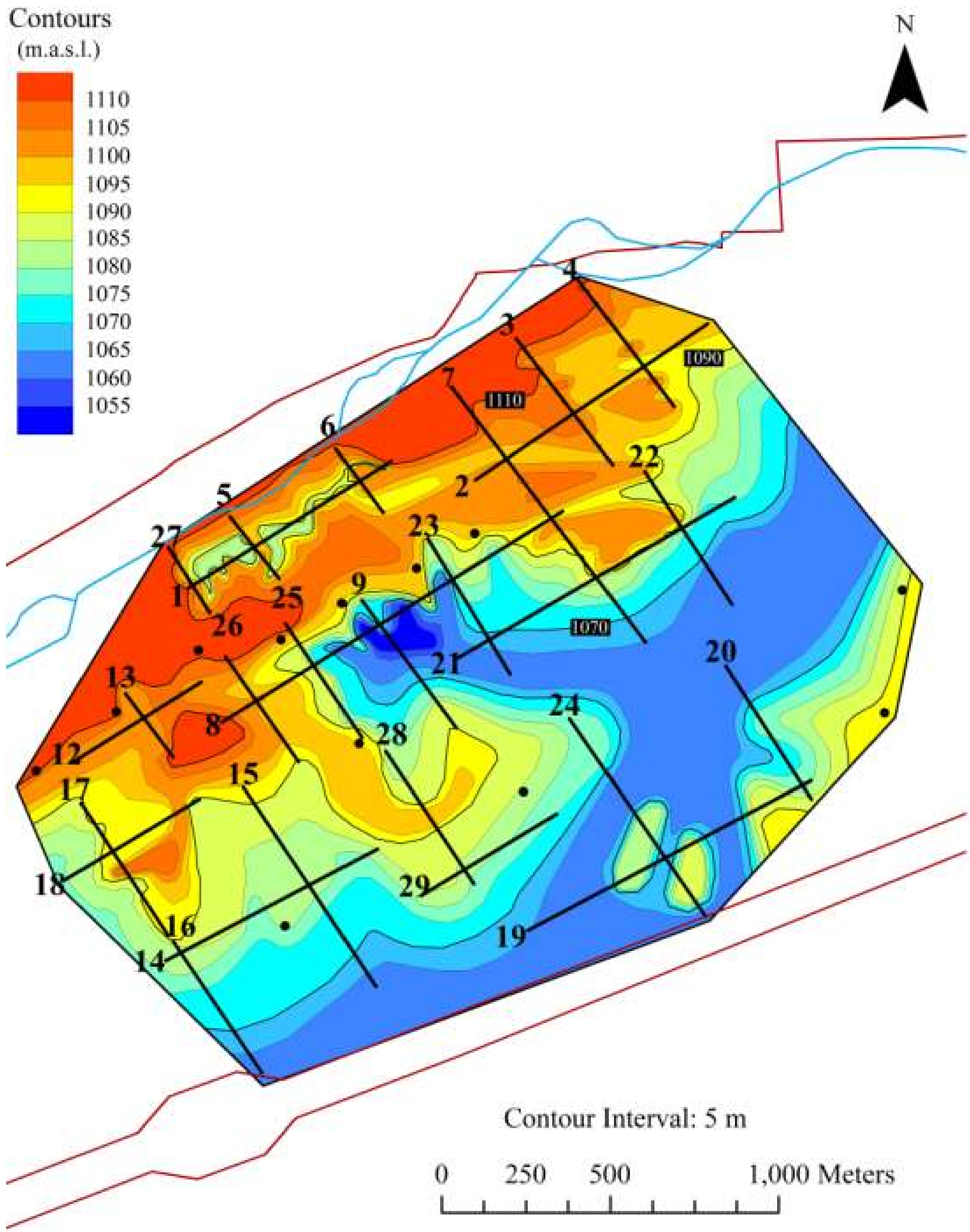
Contours
(m.a.s.l.)
1110
1105
1100
1095
1090
1085
1080
1075
1070
1065
1060
1055
N
1090
1110
1070
1
2
3
4
5
6
7
8
9
12
13
14
15
16
17
18
19
20
21
22
23
24
25
26
27
28
29
Contour Interval: 5 m
0
250
500
1,000 Meters

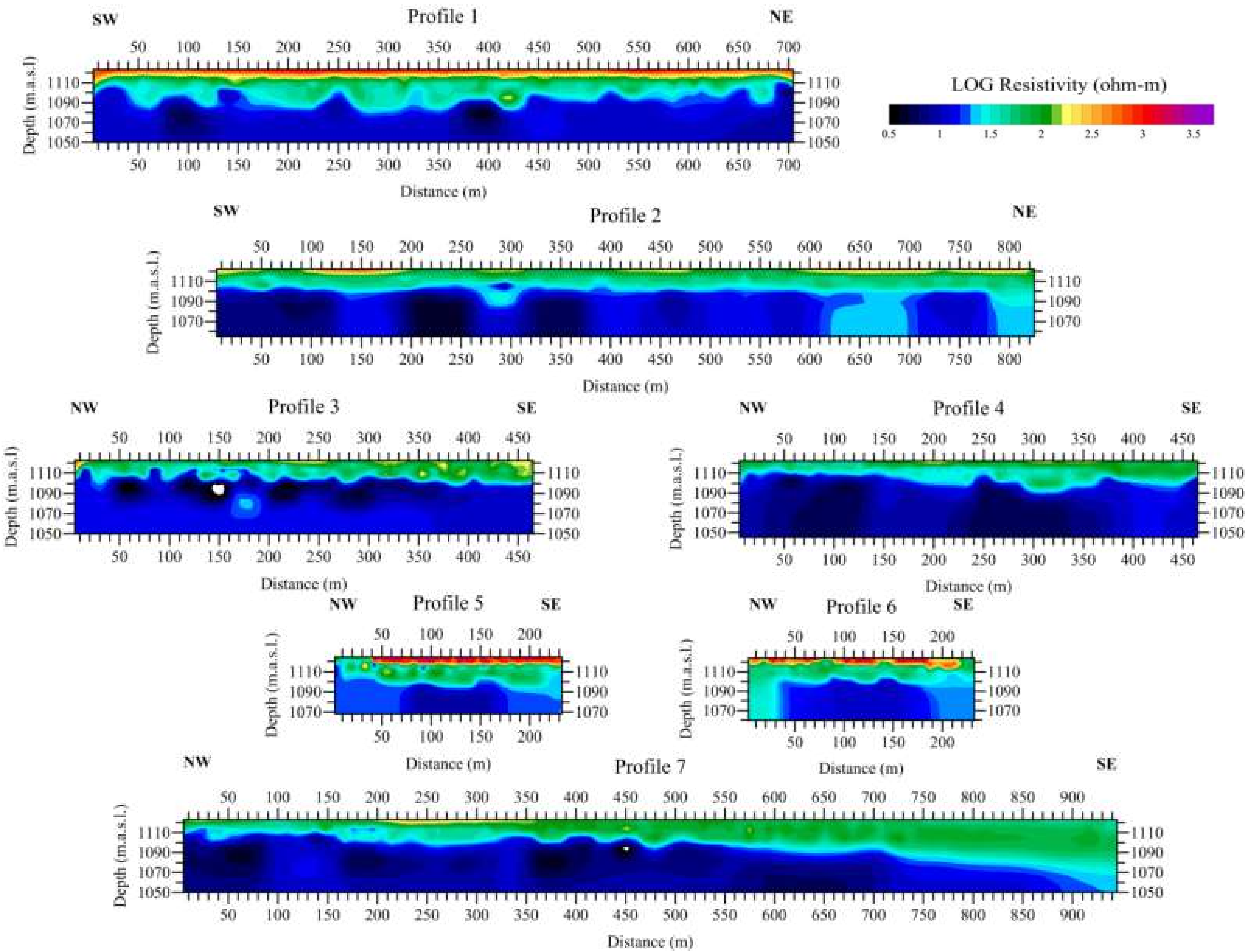
Profile 1
SW
NE
LOG Resistivity (ohm-m)
Depth (m.a.s.l)
Distance (m)
Profile 2
Profile 3
NW
SE
Profile 4
Profile 5
Profile 6
Profile 7

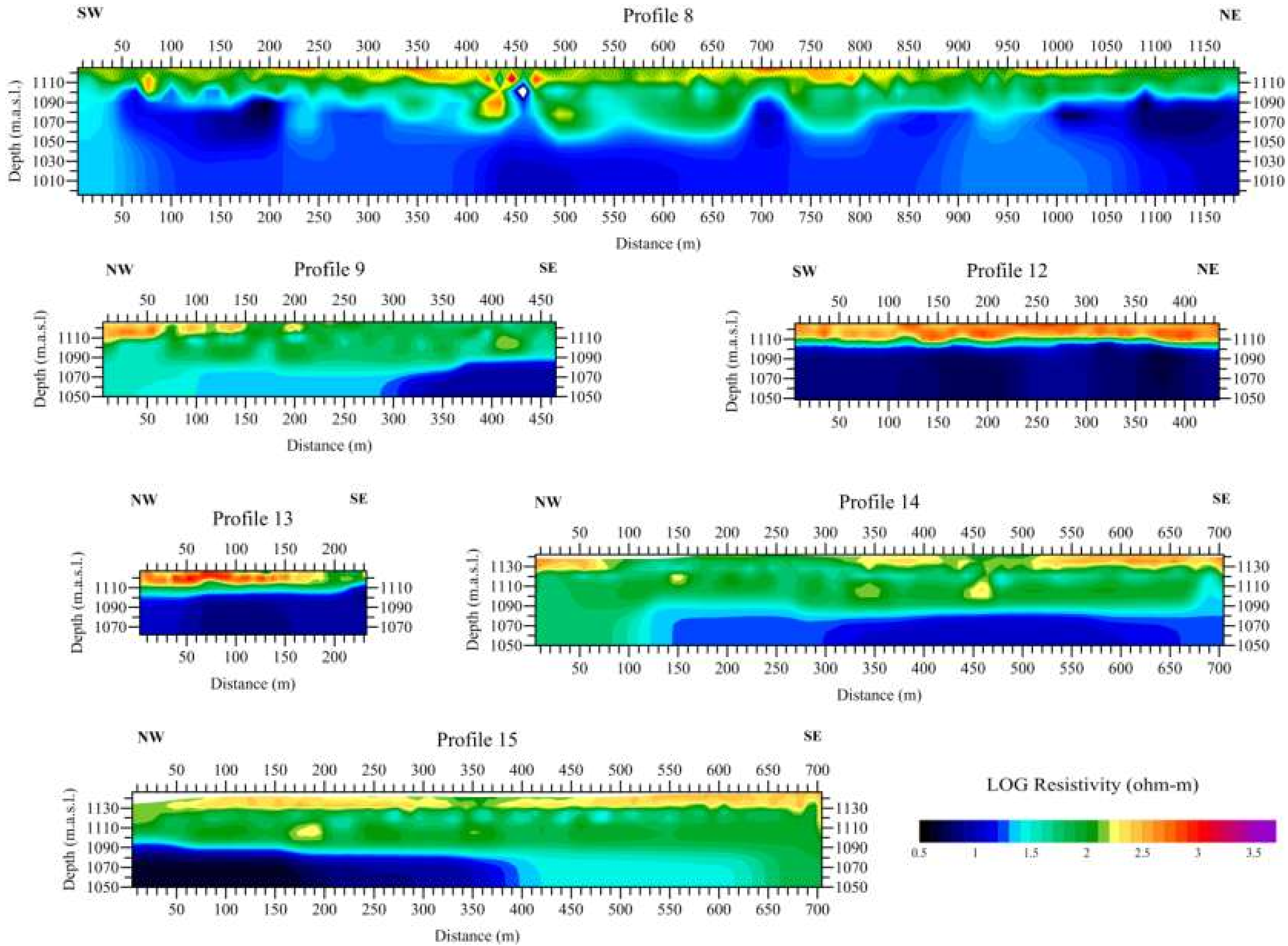
Profile 8
SW
NE
50 100 150 200 250 300 350 400 450 500 550 600 650 700 750 800 850 900 950 1000 1050 1100 1150
Depth (m.a.s.l.)
1110 1090 1070 1050 1030 1010
Distance (m)
Profile 9
NW
SE
50 100 150 200 250 300 350 400 450
Depth (m.a.s.l)
1110 1090 1070 1050
Distance (m)
Profile 12
SW
NE
50 100 150 200 250 300 350 400
Depth (m.a.s.l)
1110 1090 1070 1050
Profile 13
NW
SE
50 100 150 200
Depth (m.a.s.l.)
1110 1090 1070
Distance (m)
Profile 14
NW
SE
50 100 150 200 250 300 350 400 450 500 550 600 650 700
Depth (m.a.s.l.)
1130 1110 1090 1070 1050
Distance (m)
Profile 15
NW
SE
50 100 150 200 250 300 350 400 450 500 550 600 650 700
Depth (m.a.s.l.)
1130 1110 1090 1070 1050
Distance (m)
LOG Resistivity (ohm-m)
0.5 1 1.5 2 2.5 3 3.5

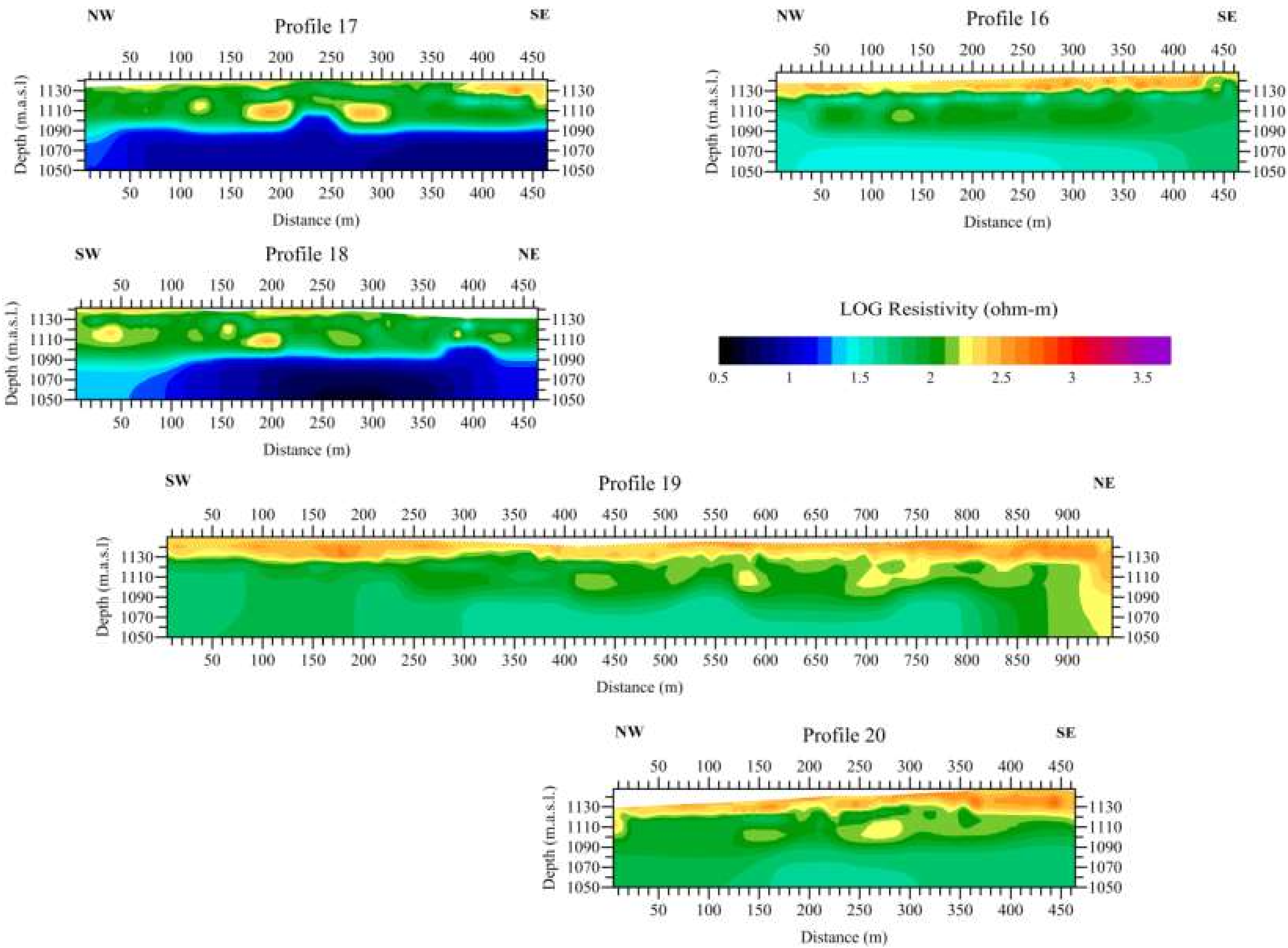
NW
Profile 17
SE
Depth (m.a.s.l)
Distance (m)
NW
Profile 16
SE
Depth (m.a.s.l.)
Distance (m)
SW
Profile 18
NE
Depth (m.a.s.l.)
Distance (m)
LOG Resistivity (ohm-m)
0.5
1
1.5
2
2.5
3
3.5
SW
Profile 19
NE
Depth (m.a.s.l)
Distance (m)
NW
Profile 20
SE
Depth (m.a.s.l.)
Distance (m)

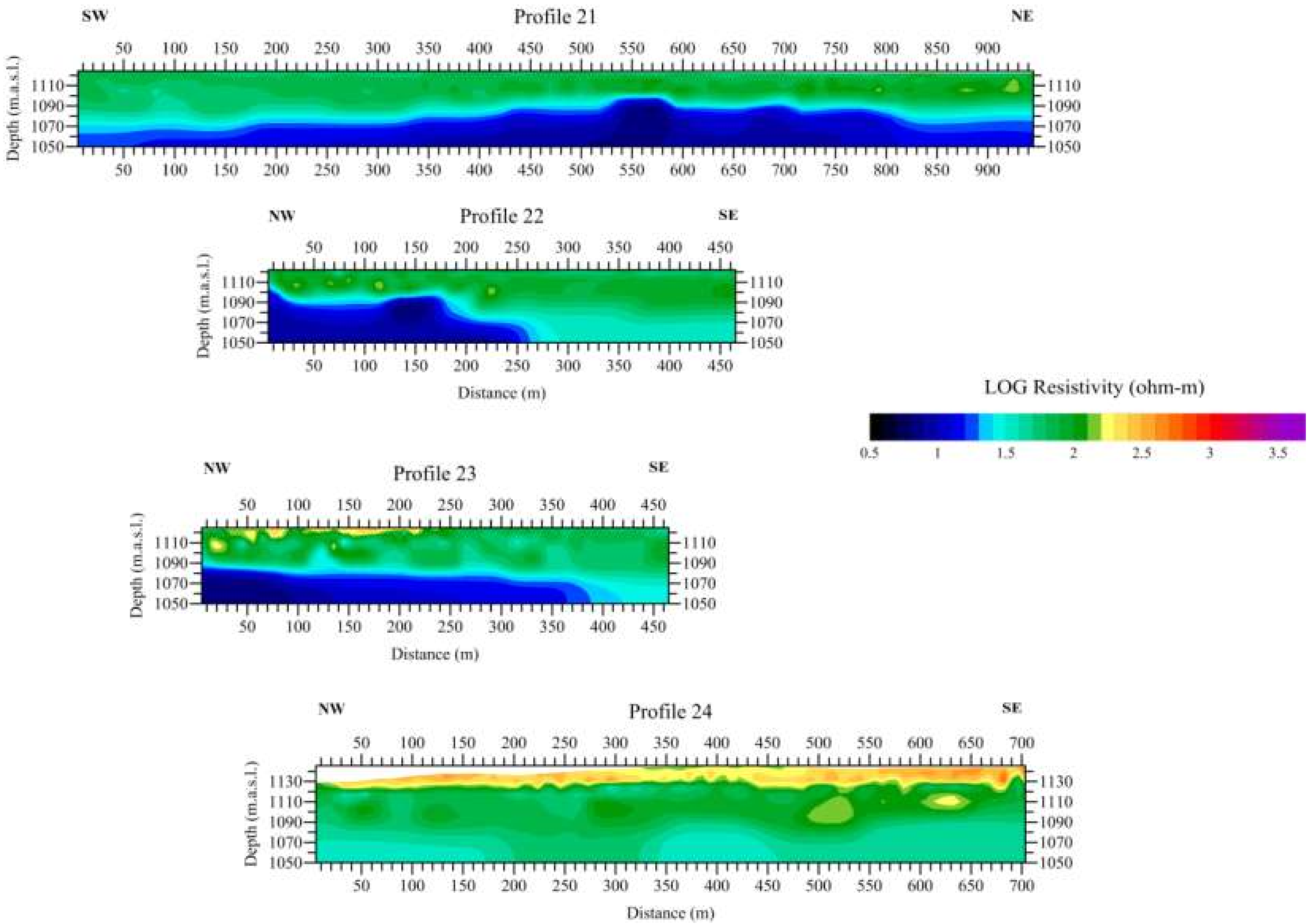
SW
Profile 21
NE
Depth (m.a.s.l.)
NW
Profile 22
SE
Depth (m.a.s.l.)
Distance (m)
LOG Resistivity (ohm-m)
0.5 1 1.5 2 2.5 3 3.5
NW
Profile 23
SE
Depth (m.a.s.l.)
Distance (m)
NW
Profile 24
SE
Depth (m.a.s.l.)
Distance (m)

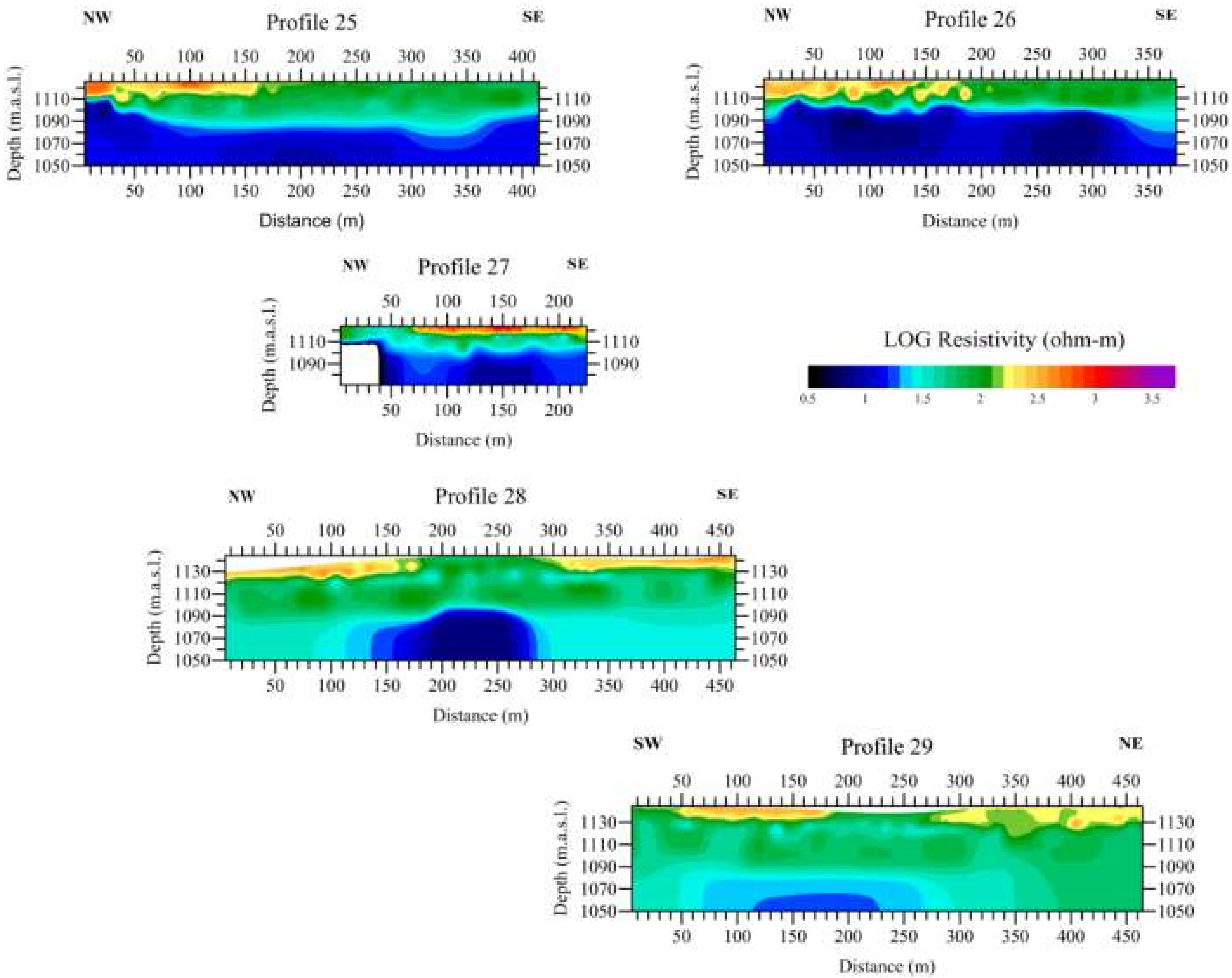
Profile 25
NW
SE
Depth (m.a.s.l.)
Distance (m)
Profile 26
NW
SE
Depth (m.a.s.l.)
Distance (m)
Profile 27
NW
SE
Depth (m.a.s.l.)
Distance (m)
LOG Resistivity (ohm-m)
0.5 1 1.5 2 2.5 3 3.5
Profile 28
NW
SE
Depth (m.a.s.l.)
Distance (m)
Profile 29
SW
NE
Depth (m.a.s.l.)
Distance (m)

Table 1. Laboratory resistivity measurements for Alluvium_T1_29-34 ft

Water Content	Sample Number	Resistivity (ohm-m)	Average (ohm-m)	Standard Deviation
0.03	1	389.16		
0.03	2	276.22	360.59	74.33
0.03	3	416.40		
0.06	1	198.48		
0.06	2	315.35	223.92	81.73
0.06	3	157.94		
0.09	1	199.73		
0.09	2	172.63	165.06	39.00
0.09	3	122.84		
0.12	1	56.45		
0.12	2	82.77	69.58	13.16
0.12	3	69.52		
0.15	1	57.32		
0.15	2	61.42	58.74	2.32
0.15	3	57.47		

Table 2. Laboratory resistivity measurements for Alluvium_T1_39-44 ft

Water Content	Sample Number	Resistivity (ohm-m)	Average (ohm-m)	Standard Deviation
0.03	1	215.93		
0.03	2	315.65	274.61	52.15
0.03	3	292.24		
0.06	1	211.18		
0.06	2	207.59	237.55	48.82
0.06	3	293.89		
0.09	1	143.00		
0.09	2	138.27	158.88	31.68
0.09	3	195.35		
0.12	1	59.65		
0.12	2	90.26	78.61	16.56
0.12	3	85.93		
0.15	1	65.40		
0.15	2	60.83	63.29	2.31
0.15	3	63.64		

Table 3. Laboratory resistivity measurements for Alluvium_T1_49-54 ft

Water Content	Sample Number	Resistivity (ohm-m)	Average (ohm-m)	Standard Deviation
0.03	1	296.94		
0.03	2	378.49	370.96	70.56
0.03	3	437.46		
0.06	1	172.47		
0.06	2	317.66	214.85	89.50
0.06	3	154.41		
0.09	1	74.33		
0.09	2	65.99	72.09	5.35
0.09	3	75.96		
0.12	1	57.00		
0.12	2	54.35	55.64	1.33
0.12	3	55.57		
0.15	1	51.48		
0.15	2	52.65	53.28	2.19
0.15	3	55.72		

Table 4. Laboratory resistivity measurements for Alluvium_T2_14-19 ft

Water Content	Sample Number	Resistivity (ohm-m)	Average (ohm-m)	Standard Deviation
0.03	1	433.75		
0.03	2	688.81	621.17	164.38
0.03	3	740.93		
0.06	1	316.40		
0.06	2	433.75	416.21	92.30
0.06	3	498.47		
0.09	1	288.41		
0.09	2	218.01	239.14	42.82
0.09	3	210.98		
0.12	1	111.33		
0.12	2	152.94	144.98	30.45
0.12	3	170.66		
0.15	1	95.69		
0.15	2	102.96	106.17	12.39
0.15	3	119.85		

Table 5. Laboratory resistivity measurements for Alluvium_T2_24-29 ft

Water Content	Sample Number	Resistivity (ohm-m)	Average (ohm-m)	Standard Deviation
0.03	1	355.32		
0.03	2	352.41	354.35	1.68
0.03	3	355.32		
0.06	1	182.38		
0.06	2	166.71	193.34	33.48
0.06	3	230.92		
0.09	1	99.97		
0.09	2	121.63	121.48	21.44
0.09	3	142.85		
0.12	1	90.94		
0.12	2	100.59	97.87	6.04
0.12	3	102.07		
0.15	1	95.69		
0.15	2	98.51	95.94	2.46
0.15	3	93.61		

Table 6. Laboratory resistivity measurements for Alluvium_T2_34-39 ft

Water Content	Sample Number	Resistivity (ohm-m)	Average (ohm-m)	Standard Deviation
0.03	1	264.54		
0.03	2	239.92	246.79	15.50
0.03	3	235.92		
0.06	1	157.78		
0.06	2	154.09	156.14	1.88
0.06	3	156.55		
0.09	1	107.48		
0.09	2	117.83	114.99	6.56
0.09	3	119.65		
0.12	1	86.38		
0.12	2	82.49	85.78	3.03
0.12	3	88.47		
0.15	1	84.88		
0.15	2	71.80	77.78	6.61
0.15	3	76.66		

Table 7. Laboratory resistivity measurements for Eolian_S1

Water Content	Sample Number	Resistivity (ohm-m)	Average (ohm-m)	Standard Deviation
0.03	1	230.32		
0.03	2	265.99	252.15	19.13
0.03	3	260.14		
0.06	1	83.09		
0.06	2	84.13	89.86	10.84
0.06	3	102.37		
0.09	1	66.91		
0.09	2	66.02	69.53	5.33
0.09	3	75.66		
0.12	1	61.12		
0.12	2	39.34	53.17	12.03
0.12	3	59.06		
0.15	1	54.55		
0.15	2	42.12	47.09	6.58
0.15	3	44.60		
0.20	1	29.19		
0.20	2	28.46	29.50	1.23
0.20	3	30.86		

Table 8. Laboratory resistivity measurements for Eolian_S2

Water Content	Sample Number	Resistivity (ohm-m)	Average (ohm-m)	Standard Deviation
0.03	1	273.46		
0.03	2	280.89	262.29	26.06
0.03	3	232.50		
0.06	1	101.61		
0.06	2	95.44	101.51	6.02
0.06	3	107.48		
0.09	1	64.07		
0.09	2	71.36	68.68	4.01
0.09	3	70.62		
0.12	1	51.40		
0.12	2	54.20	53.56	1.92
0.12	3	55.09		
0.15	1	44.75		
0.15	2	57.44	49.22	7.13
0.15	3	45.48		
0.20	1	38.48		
0.20	2	39.20	39.25	0.80
0.20	3	40.07		

Table 9. Laboratory resistivity measurements for Eolian_S3

Water Content	Sample Number	Resistivity (ohm-m)	Average (ohm-m)	Standard Deviation
0.03	1	274.05		
0.03	2	257.93	262.76	9.81
0.03	3	256.32		
0.06	1	108.64		
0.06	2	94.50	108.11	13.35
0.06	3	121.19		
0.09	1	65.69		
0.09	2	77.71	68.13	8.63
0.09	3	60.98		
0.12	1	43.70		
0.12	2	45.88	44.87	1.10
0.12	3	45.01		
0.15	1	30.71		
0.15	2	34.31	33.55	2.54
0.15	3	35.61		
0.20	1	28.84		
0.20	2	28.35	27.60	1.73
0.20	3	25.63		

Table 10. Laboratory resistivity measurements for Eolian_S4

Water Content	Sample Number	Resistivity (ohm-m)	Average (ohm-m)	Standard Deviation
0.03	1	324.42		
0.03	2	248.34	282.03	38.78
0.03	3	273.32		
0.06	1	121.32		
0.06	2	122.23	116.31	9.48
0.06	3	105.38		
0.09	1	58.92		
0.09	2	58.92	63.82	8.50
0.09	3	73.64		
0.12	1	43.70		
0.12	2	45.45	45.14	1.31
0.12	3	46.28		
0.15	1	35.86		
0.15	2	40.08	37.43	2.31
0.15	3	36.33		
0.20	1	25.48		
0.20	2	23.77	25.40	1.60
0.20	3	26.96		

Table 11. Laboratory resistivity measurements for T1_57ft_Sandy_Clay

Water Content	Sample Number	Resistivity (ohm-m)	Average (ohm-m)	Standard Deviation
0.25	1.1	16.45		
0.25	2.1	13.49	14.51	1.68
0.25	3.1	13.60		
0.25	1.2	14.69		
0.25	2.2	15.59	15.12	0.45
0.25	3.2	15.08		

Table 12. Laboratory resistivity measurements for T1_75ft_Silty_Clay

Water Content	Sample Number	Resistivity (ohm-m)	Average (ohm-m)	Standard Deviation
0.25	1.1	15.85		
0.25	2.1	13.45	15.36	1.72
0.25	3.1	16.80		
0.25	1.2	15.56		
0.25	2.2	16.08	16.01	0.43
0.25	3.2	16.41		

Table 13. Laboratory resistivity measurements for T1_80ft_Clay

Water Content	Sample Number	Resistivity (ohm-m)	Average (ohm-m)	Standard Deviation
0.25	1.1	13.44		
0.25	2.1	16.90	15.93	2.17
0.25	3.1	17.45		
0.25	1.2	15.64		
0.25	2.2	12.99	14.34	1.33
0.25	3.2	14.37		